Chapter 2

Structure based design and virtual screening of indole scaffolds targeting Plasmodium falciparum: an experimental and computational approach for antimalarial drug discovery

2.1 Introduction

The transmission of malaria occurs when infected female Anopheles mosquitoes bite humans, transmitting the Plasmodium parasites responsible for the disease. Approximately 247 million malaria cases were recorded globally in 2021, leading to 625,000 fatalities. Most of these fatalities took place in sub-Saharan Africa, where malaria is highly common.[135] The development of antimalarial medications has been vital in decreasing the morbidity and mortality rates associated with malaria. However, drug-resistant Plasmodium strains, particularly in Southeast Asia, undermine the efficacy of current antimalarial drugs.[136] As a result, the critical importance of developing new and effective drugs to combat malaria remains at the forefront of global health concerns.

The discovery and development of new antimalarial drugs have made significant strides in the past decade. The identification of new drug targets and the design of novel chemical scaffolds have been made possible by advances in genomics, high-throughput screening, and structural biology.

Indole is a heterocyclic organic compound that has been widely investigated in medicinal chemistry due to its diverse biological activities such as antidiabetic,[137] anticancer,[138] anti-hypertensive,[139] antimicrobial,[140] antileishmanial[141] including its potential as an antimalarial agent.[142,143] The Dd2 Plasmodium falciparum malaria strain was selectively inhibited by the Flinderoles B and C **(Fig 1, a, b, c)** isolated from Flindersia amboinensis (IC50 values range = 0.15-1.42 μM).[144] Likewise, NITD609, **(Fig 1, d)** a substance from the Spiro indolone class that has been proposed as an antimalarial drug and is currently undergoing clinical studies (displaying IC50 = 10 nM toward P. falciparum).[145,146] Luthra *et al* designed melatonin like structures and developed a new class of antimalarials based on aryl alkane imino tryptamine derivatives **(Fig 1, e)**. Various compounds with anti-malarial properties have been discovered in the low micromolar/high nanomolar range. These compounds are effective in inhibiting the erythrocytic cycle during the trophozoite

stage and can also synchronize parasite populations by blocking melatonin-induced growth. Some compounds exhibited the capability to interact with MT1 (human melatonin receptor).[147]

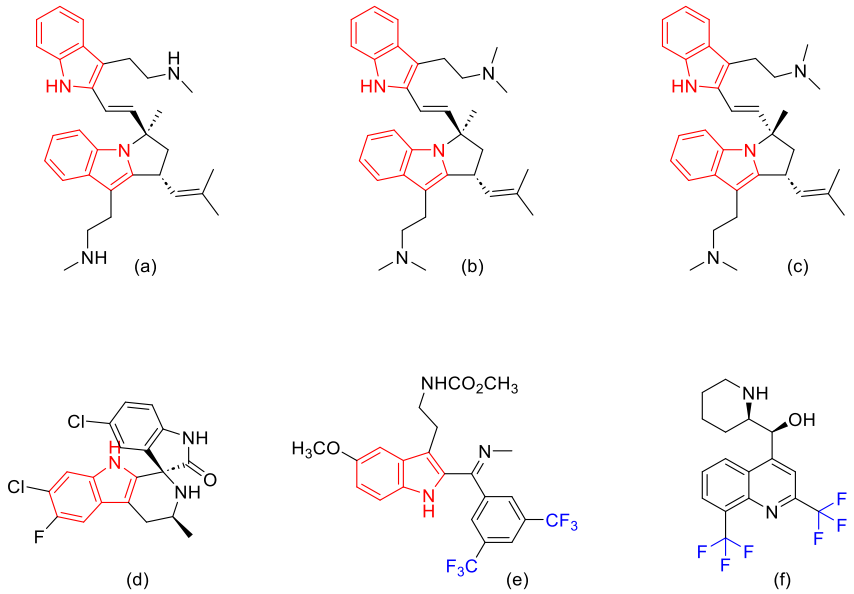

Figure 1: (a) Flinderoles-A (b) Flinderoles-B (c) Flinderoles-C (d) Spiroindolone NITD609 (e) melatonin like antimalarial indole scaffold (f) Mefloquine antiparasitic drug to treat malaria

Mutation in specific target proteins is a frequently used strategy by Plasmodium to develop resistance against antimalarial drugs. Plasmodium falciparum dihydrofolate reductase gene (PfDHFR) encodes the dihydrofolate reductase (DHFR) enzyme, which is the target of interest. The active site of PfDHFR is a particular area in the enzyme where the catalytic reaction occurs. Using NADPH as a cofactor, the active site of PfDHFR converts dihydrofolate (DHF) into tetrahydrofolate (THF).[148] The active site of PfDHFR may exhibit variations in the amino acid residues present, but certain key residues that contribute to its catalytic function have been pinpointed. Some of the amino acid residues commonly found in the active site of the enzyme include Trp48, Met49, Asn51, Phe58, Ser108, Ile164, and Asp54, among others.[149,150] For the enzyme to catalyze the reduction reaction, these residues play a critical role in binding and interacting with the substrate and cofactor molecules. A thorough understanding of the active site in PfDHFR has been key in the development of antimalarial drugs. The active site of PfDHFR is the focus of

inhibitors designed to inhibit enzyme function and impede the growth of the malaria parasite.

A library containing 35 compounds, which are derived from indole, was designed to predict potential malaria inhibitors. We identified 10 active scaffolds from this and synthesized them using the materials that were readily available. To characterize the synthesized compounds, ^{1}H NMR, mass spectroscopy, and FT-IR techniques were employed. To strengthen our findings, we conduct both in silico and in vitro analyses on the synthesized compounds to evaluate their activity against the plasmodium falciparum parasite. The docking study was conducted on the wild-type PfDHFR-TS, and the results indicate that the synthesized compounds had significantly lower binding energy affinity compared to the standard chloroquine. In this study, we aimed to investigate the antimalarial activity of a series of indole derivatives, with a focus on the role of the trifluoromethyl (CF_3) group and melatonin like indole derivatives. Our findings have important implications for the generation of new and more effective malarial inhibitor drugs, which are essentially needed to combat the growing problem of drug resistance.

2.2 Result and Discussion

2.2.1 Chemistry

The titled compounds **9a-j** were synthesized according to route illustrated in the reaction **Scheme 1,** which were characterized by various spectroscopic methods like ^{1}H-NMR, FT-IR and mass spectroscopy. The reaction started with the formylation of indole by vilsmeier-haack reaction which was in the next step reacted with different n-phenyl propanamide derivatives to form **4a-j** in good amount of yield. In the next step ethyl cyanoacetate and hydrazine hydrate were mixed and freeze to 0°C and obtained product was poured in water and acetyl acetone was added in the presence of few drops of HCl to afford 90% yield of **6**. The compound **6** was reacted with 3,5-bistrifluoromethyl aniline to give 87% yield of cyano acetamide derivative **8**. The last step was reaction of formylated indole derivatives **4a-j** with active methylene group in cyano acetamide derivative **8** in the presence of few drops of piperidine in methanol to afford titled product **9a-j**.

The ^{1}H NMR of the final compounds proofed that the both CH_2 protons of propanamide derivatives were observed at 2.90-3.06 ppm and 4.69-4.74 ppm as triplet respectively. The proton of NH in propanamide was detected in the range of 9.30-10.19 ppm and NH proton

of cyanoacetamide was observed at 10.69-10.73 ppm. The two peaks were merged which was identified one was proton of indole C2 proton and another which is adjacent to nitrile group gives a singlet at 8.43-8.46 ppm. A doublet of CH proton next to the trifluoromethyl group observed at 8.61-8.66 ppm. The aromatic region was distinguished between 6.83-8.04 ppm.

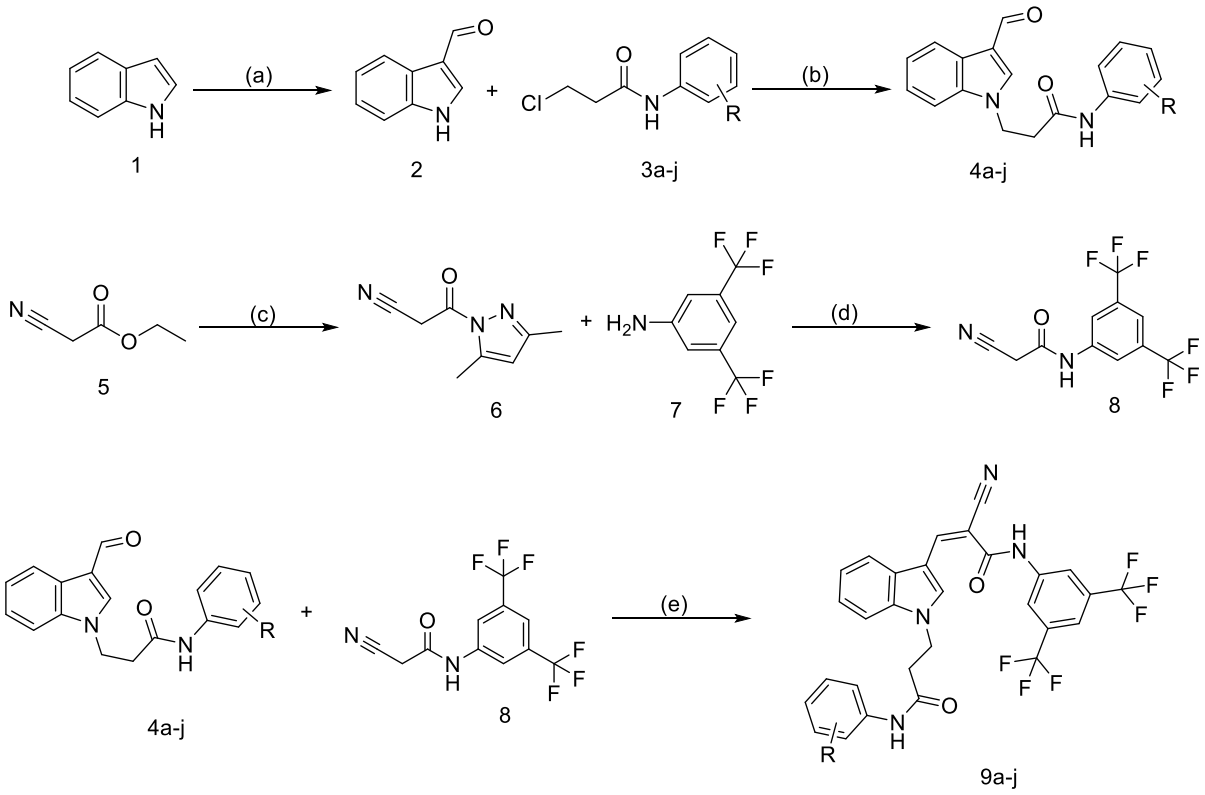

Scheme 1: Reagent and conditions: (a) Vilsmeier reaction (b) K_2CO_3, DMF, reflux (c) Hydrazine hydrate (99%), 0°C, H_2O and Acetyl acetone, HCl, H_2O, room temp. (d) Toluene, reflux (e) Piperidine, methanol, room temp.

In this study, extensive structural characterization was conducted through ^{1}H NMR, mass spectrometry, and IR spectroscopy for all ten compounds. These techniques collectively provided a robust elucidation of the molecular structures. To further substantiate the structural understanding of the most active compound (9c), a targeted ^{13}C NMR using the DEPT-135 technique was employed for differentiation between CH (methine) and CH_2 (methylene) carbon. The two negative signals of propanamide chain (CH_2) were appears at 36.91 and 43.34 ppm respectively. A positive signal at 143.63 ppm confirmed the existence of a methine carbon attached to the C3 position of indole. The presence of

carbons in aromatic rings was detected through positive signals ranging from 111.91-130.83 ppm. The physiochemical properties of the synthesized compounds **9a-j** are illustrated in **Table 1**.

Table 1: Physiochemical characteristics of (3,5-bis(trifluoromethyl)-1*H*-indol-3-yl)-2-cyanoacrylamide derivatives 9a-j

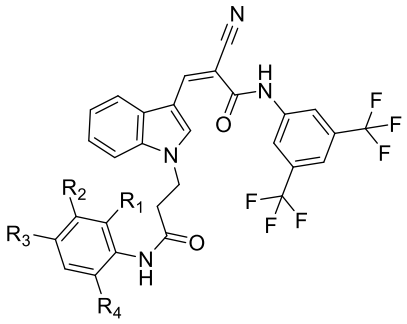

Sample code	R_1	R_2	R_3	R_4	Molecular weight	Molecular formula	Yield (%)	Melting point (°C)
9a	H	H	Br	H	649.39	$C_{29}H_{19}BrF_6N_4O_2$	87	214-216
9b	CH_3	H	CH_3	H	598.55	$C_{31}H_{24}F_6N_4O_2$	86	234-236
9c	H	Cl	H	H	604.94	$C_{29}H_{19}ClF_6N_4O_2$	90	212-214
9d	H	H	OCH_3	H	600.52	$C_{30}H_{22}F_6N_4O_3$	83	212-214
9e	H	H	F	H	588.49	$C_{29}H_{19}F_7N_4O_2$	81	237-239
9f	H	H	Cl	H	604.94	$C_{29}H_{19}ClF_6N_4O_2$	88	226-228
9g	CH_3	H	H	CH_3	598.18	$C_{31}H_{24}F_6N_4O_2$	89	244-246
9h	F	H	H	H	588.49	$C_{29}H_{19}F_7N_4O_2$	78	220-222
9i	CH_3	H	H	H	584.52	$C_{30}H_{22}F_6N_4O_2$	84	208-210
9j	H	H	CH_3	H	584.52	$C_{30}H_{22}F_6N_4O_2$	83	227-229

2.2.2 Malaria inhibitor prediction

The indole-based structures were designed for prediction of their malarial inhibitory activity and total of 35 compounds were designed to predict that compounds are active or inactive against plasmodium falciparum as depicted in **Figure 2**.

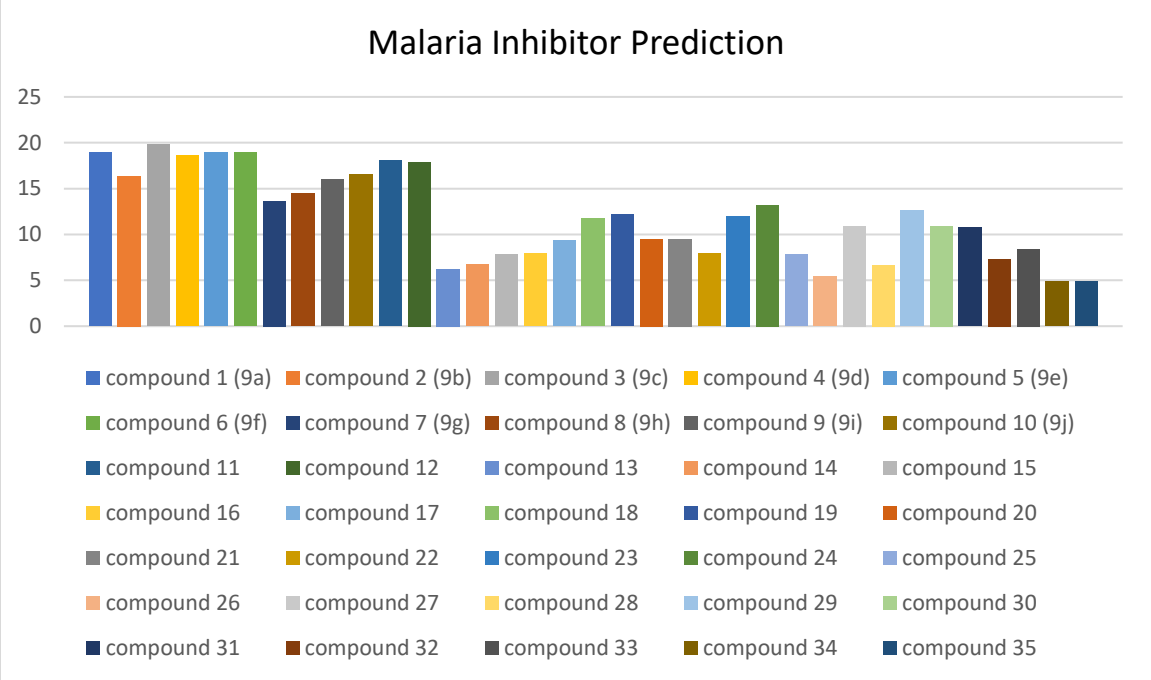

Figure 2: Malaria Inhibitor Prediction (MAIP) generated score for designed 35 indole scaffolds

Based on the generated data, **compound 3 (9c)** demonstrated exceptional activity against malaria at the blood stage, with a score of 19.7995, surpassing other designed compounds. The **compound 1** (**9a**), **compound 5** (**9e**) and **compound 6** (**9f**) show the similar activity by scoring 18.9709. The least active compound against malaria was found to be **34** and **35** which has only 4.8984 score. From the obtained data it was clear that CF_3 group has significant activity against malaria rather than trichloro, trimethyl or any other substitution. The effect of chain shortening and elongation shows the decrease in the activity at NH position of indole. The substitution at 1,3,5-tri positions were showed crucially downfall in activity. Therefore, by the following results we decided to synthesize the indole scaffold with trifluoromethyl group with cyanoacetamide chain for better activity. The molecular structures of the designed molecules can be found in **Figure 3**. The graphical representation of the structural activity relationship, based on the data acquired from MAIP, is depicted in **Figure 4**.

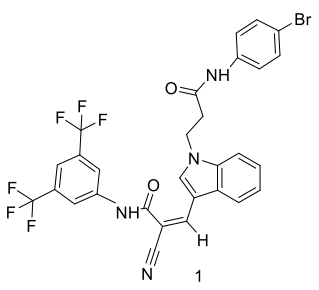
1

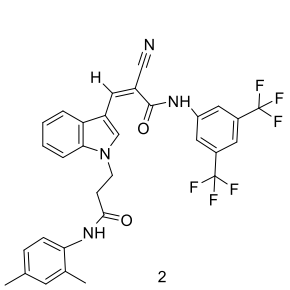
2

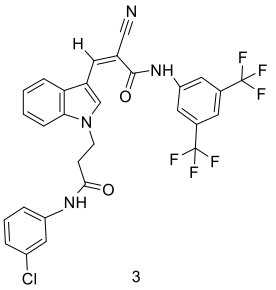
3

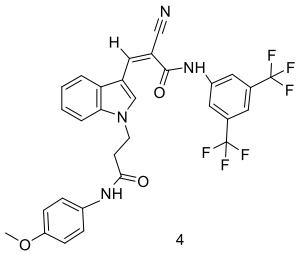
4

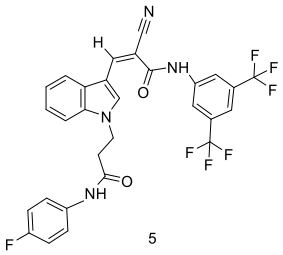
5

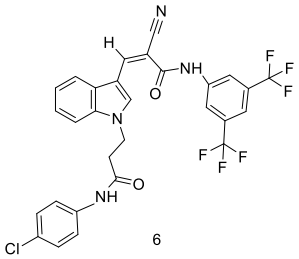
6

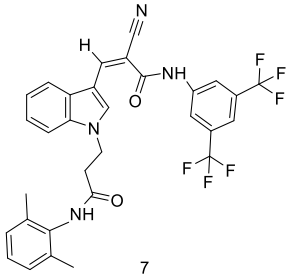
7

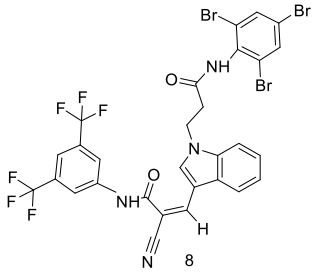
8

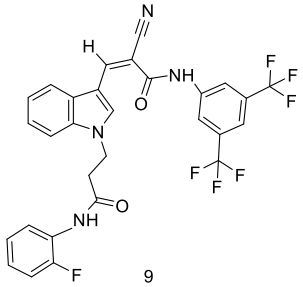
9

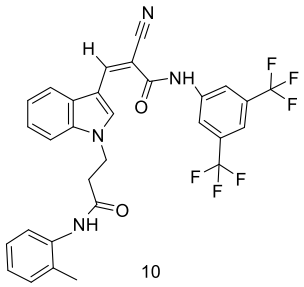
10

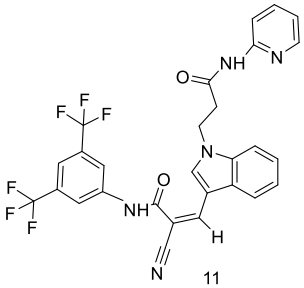
11

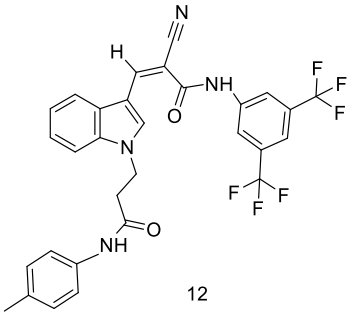
12

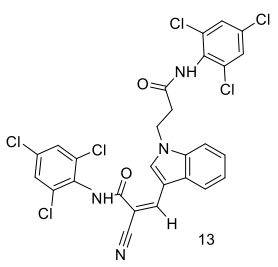
13

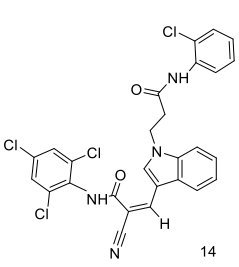
14

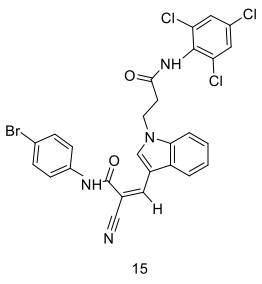
15

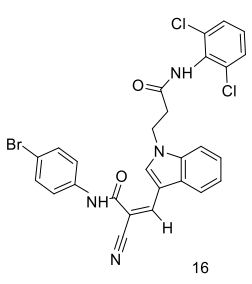
16

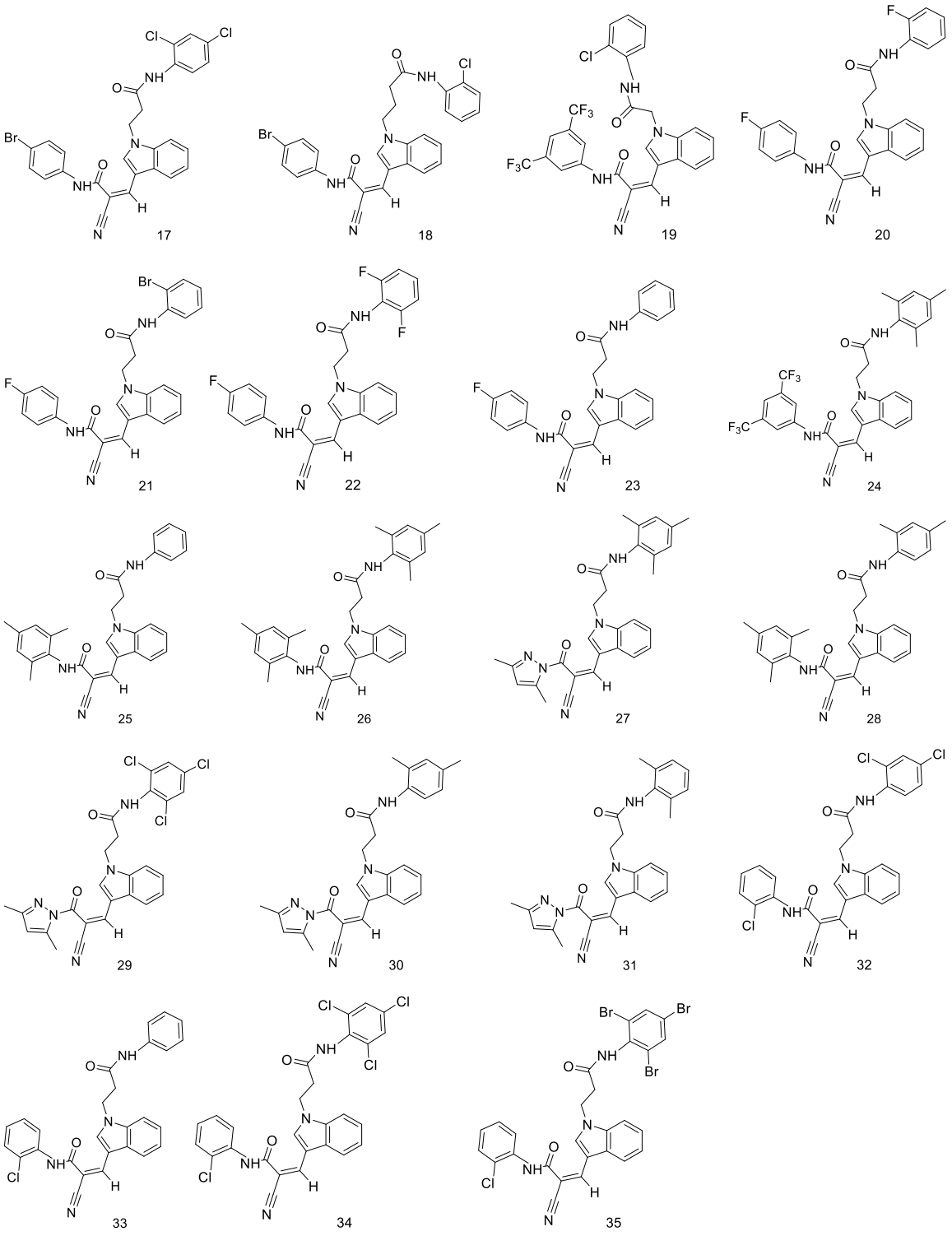

Figure 3: Indole based designed 35 compounds library

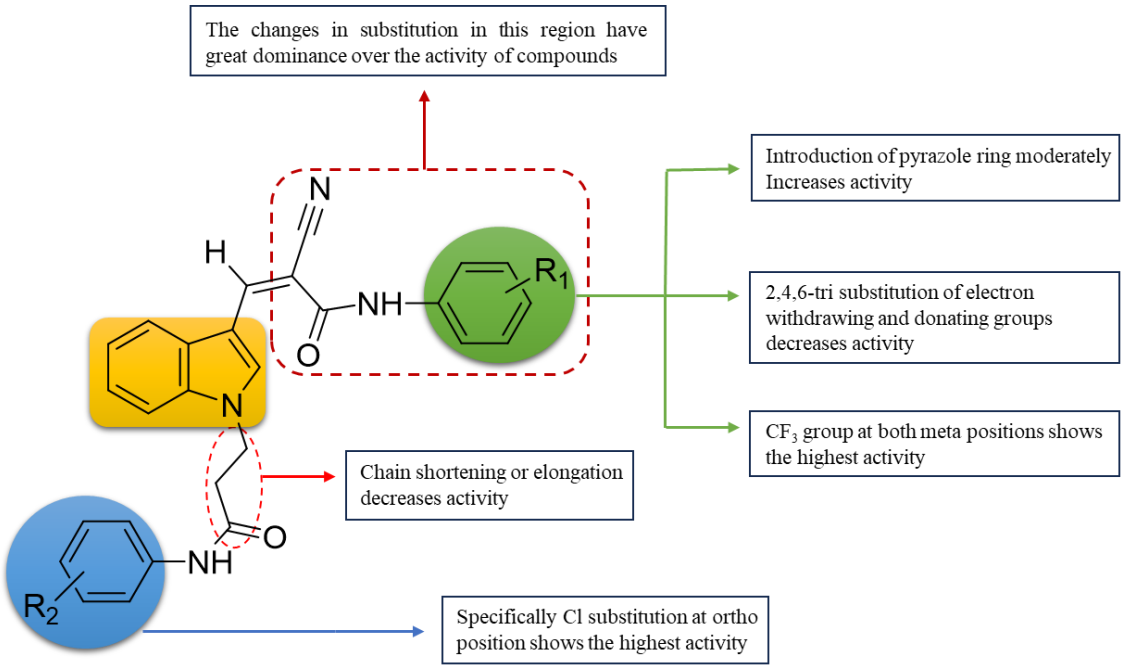

Figure 4: Structural activity relationship data for indole scaffolds obtained from the MAlaria inhibitor prediction (MAIP)

2.2.3 *In vitro* antimalarial screening

In this study we evaluated the *in vitro* antimalarial activity of a series of novel compounds against Plasmodium falciparum. A standard drug chloroquine was used as positive control for comparison. The compounds revealed varying degrees of antimalarial activity, as suggested by their inhibitory effects on parasite growth. The experimental protocols result is depicted in **Table 2**.

Table 2: IC_{50} values of synthesized compounds 9a-j against plasmodium falciparum

Entry	IC_{50} (µg/ml)
9a	089 ± 0.003
9b	1.01 ± 0.001
9c	0.79 ± 0.005
9d	0.97 ± 0.002
9e	0.88 ± 0.001
9f	0.84 ± 0.004
9g	0.92 ± 0.005
9h	0.95 ± 0.003
9i	1.05 ± 0.002
9j	1.03 ± 0.002
Chloroquine	0.020 ± 0.004

Few of the synthesized compounds showed moderate to good antimalarial activity. Specifically highest active compound was found to be **9c** with 0.79 µg/ml IC_{50} value, the possible reason should be chloro substitution on *meta* position at propanamide induced ring and even the attachment of chloro group at *para* position shows good activity. The compound **9e**, **9a** and **9g** also exhibit good activity. The higher IC_{50} values observed for the tested compounds, in contrast with chloroquine denoted moderate dominance however it is important to point out this result in context of potential alternative mechanisms and targets. While chloroquine acts by inhibiting heme polymerization within the parasite food vacuole[151]. It is possible that the compounds target alternative pathways or proteins involved in the parasite's life cycle, metabolism or cellular processes. The further investigation is merited for plasmodium falciparum dihydrofolate reductase enzyme which is involved in folate metabolism pathway.

2.2.4 Molecular modeling against PfDHFR

In this investigation, we performed docking studies of Chloroquine and compound **9a-j** with the Plasmodium falciparum dihydrofolate reductase (PfDHFR) using the crystal structure with PDB ID: 3QGT.[152] The docking scores and key interactions for each compound are summarized in the **Table 3**.

Table 3: Docking Results and Interactions of Compounds with Plasmodium falciparum dihydrofolate reductase (PfDHFR)

Molecule	Binding affinity	Key interactions (H-bonds)	Non-covalent interactions (fluorine interaction)
9a	-10.0	SER111, SER108	GLY44, ILE164
9b	-10.9	SER108	LEU40
9c	-10.4	SER108	GLY44, VAL45, ILE164
9d	-10.9	SER108, SER167	LEU40
9e	-10.6	SER108, SER111	ILE164
9f	-10.1	SER108	ILE164
9g	-11.1	SER108, SER111, LEU 46	SER111, LEU46
9h	-10.5	SER108, SER111, ASP54	ILE14, ILE164
9i	-10.6	SER108, SER111, ASP54	ILE164
9j	-10.5	SER108	GLY44, ILE164
Chloroquine	-7.1	SER111, ILE164	-

Upon analyzing the docking results, it is evident that all the compounds exhibited favorable binding affinity to PfDHFR, as indicated by their negative docking scores. Notably, Chloroquine displayed a docking score of -7.1 kcal/mol and formed hydrogen bonds with residues SER111 and ILE164. This suggests potential interactions between Chloroquine and the active site of PfDHFR. Compounds **9a-j** also demonstrated strong binding affinities, with docking scores ranging from -10.0 to -11.1 kcal/mol. These compounds primarily formed hydrogen bonds with various residues, including SER108, SER111, SER167, ASP54, LEU46, ALA16, and TRP48. These interactions indicate the potential involvement of specific amino acid residues in stabilizing the compound-receptor complex. Furthermore, a few compounds such as **9d**, **9e**, **9h** and **9i** exhibited additional hydrogen bonds with multiple residues, suggesting the formation of intricate networks of interactions within the active site of PfDHFR.

The interaction of trifluoromethyl group (halogen interaction) has significant role in binding with numerous amino acids which are ILE164, GLY44 and LEU40. The high electronegativity of fluorine atom reinforces the electron density which increase the electrostatic interactions inducing a more stable complex. The observed key interactions highlight the significance of hydrogen bonding in the binding of these compounds to PfDHFR. Hydrogen bonds formed with residues such as SER108, SER111, and ASP54 are likely crucial for stabilizing the compound-receptor complex and influencing their binding affinity. These docking results are consistent with previous studies on PfDHFR inhibitors, validating the reliability of our computational approach. The identified key interactions align well with the known binding modes of PfDHFR inhibitors, suggesting that these compounds have the potential to inhibit PfDHFR activity and may serve as potential antimalarial agents. The binding interactions of compound **9c, 9g** and standard drug chloroquine is visualized in **Figure 4**, **5** and **6**. An illustration of the remaining 2D binding interactions of the synthesized compounds can be found in **Figure 7**.

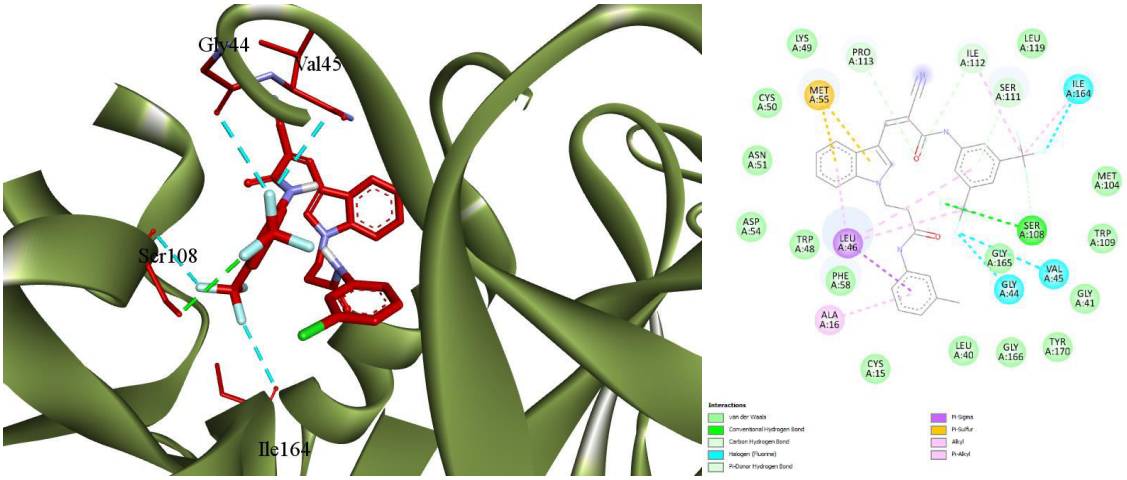

Figure 5: 3D and 2D binding interactions of compound 9c with protein 3GQT

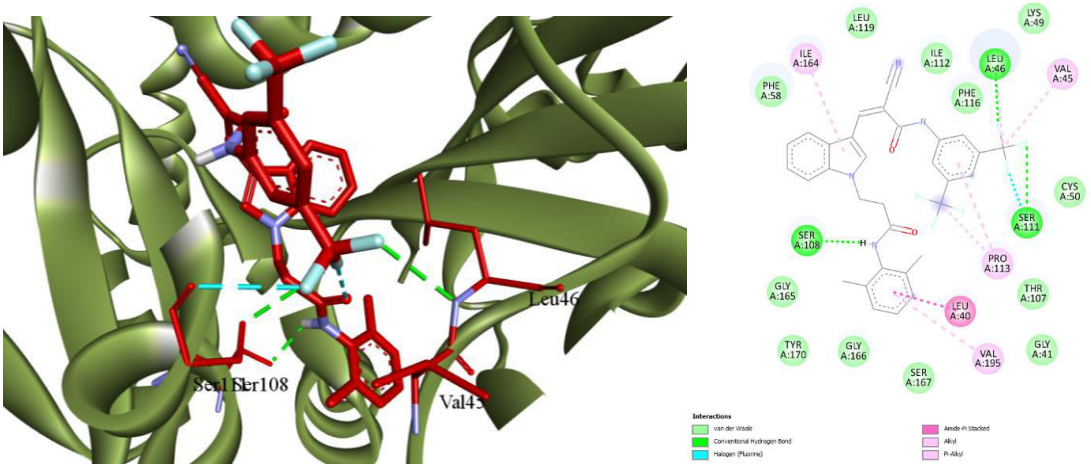

Figure 6: 3D and 2D binding interaction of compound 9g with protein 3GQT

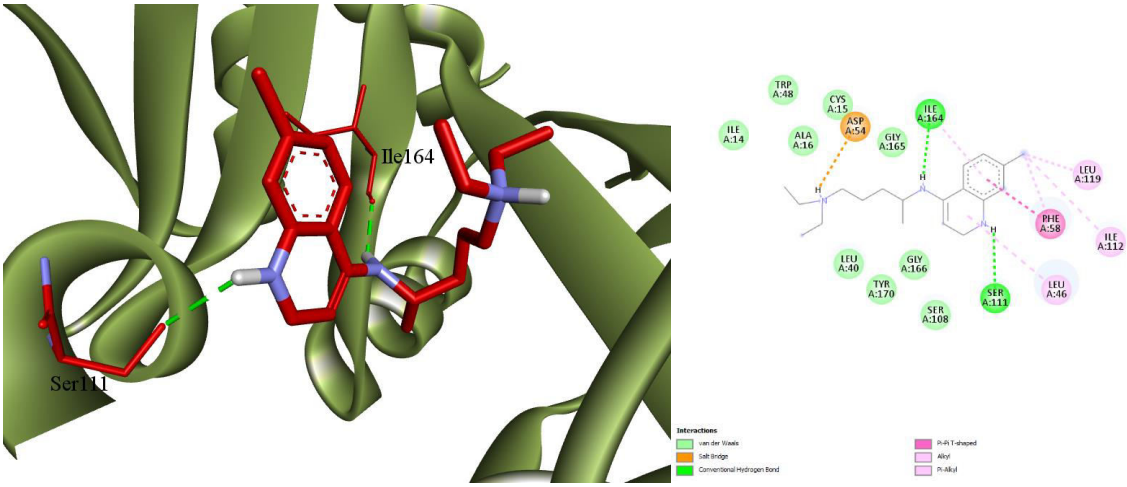

Figure 7: 3D and 2D binding interaction of chloroquine with protein 3GQT

(A)

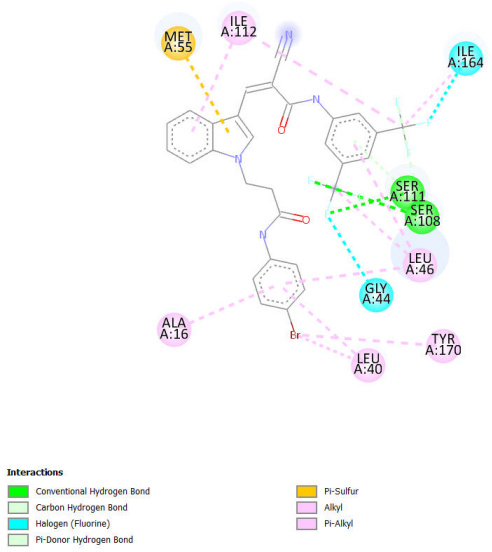

(B)

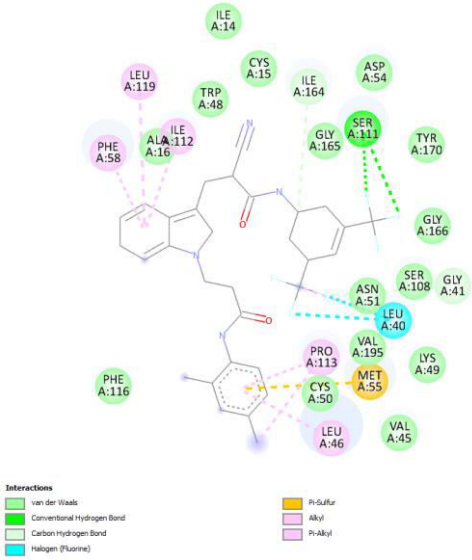

(C)

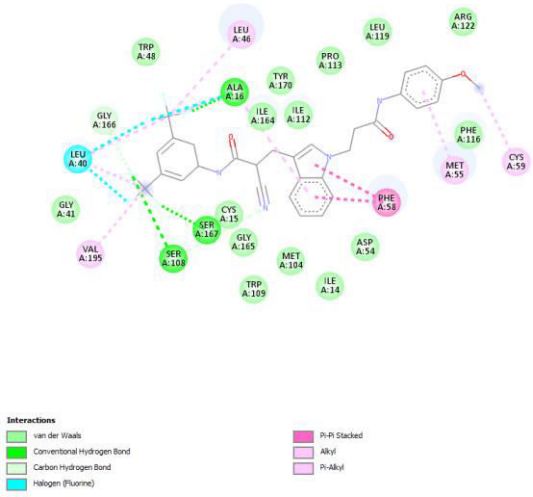

(D)

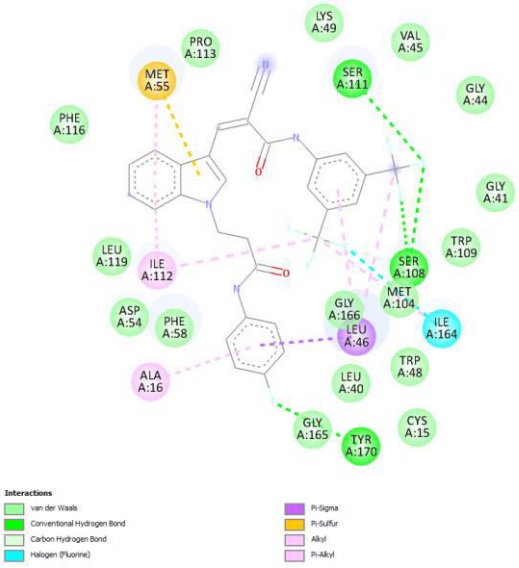

(E)

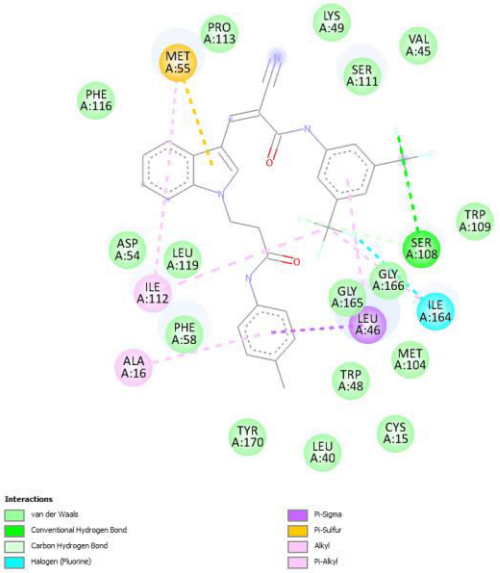

(F)

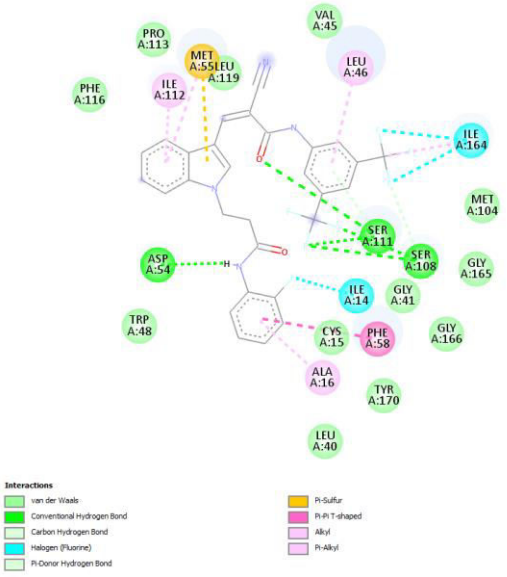

(G)

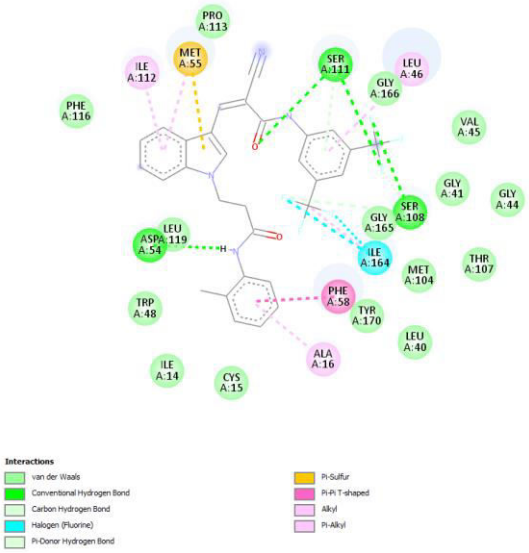

(H)

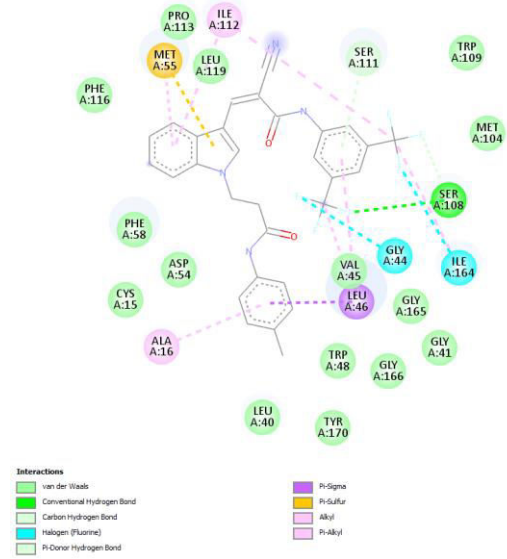

Figure 8: 2D interactions of compounds 9a (Fig. A), 9b (Fig. B), 9d (Fig. C), 9e (Fig. D), 9f (Fig. E), 9h (Fig. F) ,9i (Fig. G) and 9j (Fig. H) with protein residues

2.3 Experimental section

2.3.1 Chemistry

The chemical used in this research work were of analytical grade and used without further purifications. Phosphorus oxychloride (Cas No: 10025-87-3), sodium hydroxide (Cas No:1310-73-2), potassium carbonate (Cas No:584-08-7) and dimethyl formamide (Cas No:68-12-2) were obtained from Molychem. Ethyl cyanoacetate (Cas No:105-56-6) was procured from Chemdyes. Hydrazine hydrate (99%) (Cas No: 7803-57-8) and acetyl acetone (Cas No:123-54-6) were purchased from CDH. Piperidine (Cas No: 110-89-4) used in the experiment was obtained from the Loba chemie. 3,5-Bis(trifluoromethyl)aniline (Cas No: 328-74-5) and indole (Cas No: 120-72-9) were sourced from the Merck Millipore and spectrochem respectively. The Silica Gel 60 F_{254} TLC Aluminum Sheets (Merck KGaA, Darmstadt Germany) were used for thin-layer chromatography and spots were visualized using UV light at 254 nm and 365 nm. ^{1}H NMR spectra were recorded on a Bruker AVANCE III (400 MHz) spectrometer and AvanceNeo Ascend (400MHz) in DMSO-d_6 solvent. ^{13}C NMR spectra was recorded on AvanceNeo Ascend (101MHz) spectrometer in DMSO-d_6 solvent. Chemical shifts are expressed in δ ppm downfield from Tetramethyl silane (TMS) as an internal standard. The Fourier Transform Infrared (FT-IR) spectrum was recorded using a Shimadzu FTIR-8400 spectrometer. Samples were prepared using the potassium bromide (KBr) pellet method for infrared spectroscopy. For the mass spectral analysis, a Shimadzu QP-2010 spectrometer was utilized, operating with a direct inlet method. The melting points were recorded on an electrothermal device using open capillaries and are uncorrected. Formylation of indole and preparation of 3-chloro-*N*-phenylpropanamide derivatives were carried out as reported methods.[153,154]

→ **General procedure for synthesis of 3-(3-formyl-1*H*-indol-1-yl)-*N*-phenylpropanamide 4a-j**

Formylated indole (10 mmol) and substituted 3-chloro-*N*-phenylpropanamide (12 mmol) were dissolved in DMF (10 ml) and refluxed in the presence of K_2CO_3 (15 mmol) until the TLC indicated the complete consumption of formylated indole. After complete consumption of indole reaction mixture was

poured in ice cold water and neutralized with dil. HCl solution to get the precipitates of **4a-j** which was vacuum filtered and used without further purification.

→ **General procedure for synthesis of 3-(3,5-dimethyl-1*H*-pyrazol-1-yl)-3-oxopropanenitrile 6**

Hydrazine hydrate (99%, reagent grade) (10 mmol) was added drop wise to the solution of ethyl cyanoacetate (10 mmol) and this mixture was refrigerated at 0 °C for 30 min. The white solid that appeared after a while was vacuum filtered, washed with DCM and dried to give 2-cyano acteohydrazide Intermediate. This intermediate was dissolved in water with three drops of HCl. To this solution acetyl acetone (10 mmol) was added dropwise to give 3-(3,5-dimethyl-1*H*-pyrazol-1-yl)-3-oxopropanenitrile.

→ **General procedure for synthesis of *N*-[3,5-bis(trifluoromethyl)phenyl]-2-cyanoacetamide derivatives 8**

The obtained product **6** (10 mmol) was dissolved in toluene (10 ml) and 3,5-bis(trifluoromethyl)aniline **7** (12 mmol) were refluxed for overnight. The obtained product was vacuum filtered, dried and recrystallized from ethanol.

→ **General procedure for synthesis of 2-cyano-3-{1-[3-oxo-3-(phenylamino) propyl]-1*H*-indol-3-yl}-*N*-phenyl acrylamide 9a-j**

The compound **4a-j** (10 mmol) and *N*-(3,5-bis(trifluoromethyl)phenyl)-2-cyanoacetamide **8** (12 mmol) were stirred in methanol (10 ml) at room temperature in the presence of piperidine (05 mmol). After 30 min the precipitates were fall out in the reaction mixture which was vacuum filtered, dried and recrystallized from ethanol to give pure titled compound **9a-j**.

(*Z*)-*N*-[3,5-bis(trifluoromethyl)phenyl]-3-(1-{3-[(4-bromophenyl)amino]-3-oxopropyl}-1*H*-indol-3-yl)-2-cyanoacrylamide (9a)

Greenish yellow powder, Yield: 87%, mp 214-216 °C. IR spectrum, *v*, cm^{-1}: 1697 (C=O), 2198 (CN), 3271 (-NH-). ^{1}H NMR spectrum (400 MHz, DMSO-d_6) δ, ppm: 10.70 (s,1H; NH), 10.14 (s,1H; NH), 8.62 (d, *J*= 4.6 Hz, 2H; 3,5-bis(trifluoromethyl)phenyl), 8.43 (s, 2H; indole), 8.02 (d, *J*= 7.8 Hz, 1H; indole), 7.82 (s, 1H; indole), 7.77 (d, *J*= 8.0 Hz, 1H;

3,5-bis(trifluoromethyl)phenyl), 7.55 - 7.43 (m, 4H; C_6H_4Br), 7.43 - 7.30 (m, 2H, indole), 4.71 (s, 2H; propanamide), 2.95 (s, 2H; propanamide). Found, %: C 53.66; H 2.98; N 8.65. $C_{29}H_{19}BrF_6N_4O_2$. Calculated, %: C 53.64; H 2.95; N 8.63. *M* 649.

(*Z*)-*N*-[3,5-bis(trifluoromethyl)phenyl]-2-cyano-3-(1-{3-[(2,4-dimethylphenyl) amino]-3-oxopropyl}-1*H*-indol-3-yl)acrylamide (9b)

Greenish yellow powder, Yield 86%, mp 234-236 °C. IR spectrum, *v*, cm^{-1}: 1689 (C=O), 2198 (CN), 3279 (-NH-). ^1H NMR spectrum (400 MHz, DMSO-d_6) δ, ppm: 10.7 (s, 1H; NH), 9.31 (s, 1H; NH), 8.64 (d, *J*= 13.9 Hz, 2H; 3,5-bis(trifluoromethyl)phenyl), 8.45 (s, 2H; indole), 8.03 (d, *J*= 7.7 Hz, 1H; indole), 7.84 (s, 1H; indole), 7.76 (d, *J*=7.9 Hz, 1H; 3,5-bis(trifluoromethyl)phenyl), 7.37 (p, *J*= 7.1 Hz; 2H, indole + 2,4- xylidine), 7.13 (d, *J*=8.1 Hz, 1H; indole), 6.99 - 6.88 (m, 2H; 2,4- xylidine), 4.72 (s, 2H; propanamide), 2.94 (s, 2H; propanamide), 2.21 (s, 3H; CH_3), 1.96 (s, 3H; CH_3). Found %: C 62.19; H 4.05; N 9.33. $C_{31}H_{24}F_6N_4O_2$. Calculated, %: C 62.21; H 4.04; N 9.36. *M* 598.

(*Z*)-*N*-[3,5-bis(trifluoromethyl)phenyl]-3-(1-{3-[(3-chlorophenyl)amino]-3-oxo propyl}-1*H*-indol-3-yl)-2-cyanoacrylamide (9c)

Greenish yellow powder, Yield: 90%, mp 212-214 °C. IR spectrum, *v*, cm^{-1}: 1674 (C=O), 2198 (CN), 3271 (-NH-). ^1H NMR spectrum (400 MHz, DMSO-d_6) δ, ppm: 10.70 (s, 1H; NH), 10.19 (s, 1H;NH), 8.63 (d, *J*= 4.1 Hz, 2H; 3,5-bis(trifluoromethyl)phenyl), 8.44 (s, 2H; indole), 8.02 (d, *J*= 7.7 Hz, 1H; indole), 7.83 (s, 1H; Ar-Cl), 7.80 - 7.73 (m, 2H; indole + 3,5-bis(trifluoromethyl)phenyl), 7.40 (d, *J*= 7.6 Hz, 1H; indole), 7.39 - 7.26 (m, 3H; indole+ Ar-Cl), 7.09 - 7.07 (d, 1H; Ar-Cl), 4.72 (s, 2H; propanamide), 2.97 (s, 2H; propanamide). ^{13}C NMR spectrum (101 MHz, DMSO-d_6) δc, ppm: 36.91 (C-13), 43.34 (C-12), 111.91 (C-8), 116.93 (C-23), 117.99 (C-30), 119.17 (C-21), 119.26 (C-25), 120.62 (C-6), 120.66 (C-26), 122.69 (C-5), 123.49 (C-7), 124.13 (C-28), 130.83 (C-27), 134.39 (C-2), 143.63 (C-10) Found %: C 57.63; H 3.18; N 9.29. $C_{29}H_{19}ClF_6N_4O_2$. Calculated, %: C 57.58; H 3.17; N 9.26. *M* 604.

(*Z*)-*N*-[3,5-bis(trifluoromethyl)phenyl]-2-cyano-3-(1-{3-[(4-methoxyphenyl)amino]-3-oxopropyl}-1*H*-indol-3-yl)acrylamide (9d)

Greenish yellow powder, Yield: 83%, mp 212-214 °C. IR spectrum, *v*, cm^{-1}: 1651 (C=O), 2198 (CN), 3286 (-NH-). ^1H NMR spectrum (400 MHz, DMSO-d_6) δ, ppm: 10.71 (s,1H;

NH), 9.86 (s, 1H; NH), 8.63 (d, *J*= 4.3 Hz, 2H; 3,5-bis(trifluoromethyl)phenyl), 8.44 (s, 2H; indole), 8.02 (d, *J*= 7.7 Hz, 1H, indole), 7.83 (s, 1H; 3,5-bis(trifluoromethyl)phenyl), 7.77 (d, *J*= 8.0 Hz, 1H; indole), 7.44 - 7.32 (m, 4H; indole+ Ar- OCH_3), 6.86 - 6.83 (d, 2H; Ar- OCH_3), 4.71 (s, 2H; propanamide), 3.70 (s, 3H; OCH_3), 2.91 (s, 2H; propanamide). Found %: C 60.06; H 3.73; N 9.35. $C_{30}H_{22}F_6N_4O_3$. Calculated, %: C 60.00; H 3.69; N 9.33. *M* 600.

(*Z*)-*N*-[3,5-bis(trifluoromethyl)phenyl]-2-cyano-3-(1-{3-[(4-fluorophenyl)amino]-3-oxopropyl}-1*H*-indol-3-yl)acrylamide (9e)

Greenish yellow powder, Yield: 81%, mp 237-239 °C. IR spectrum, *v*, cm^{-1}: 1651 (C=O), 2198 (CN), 3279 (-NH-). ^{1}H NMR spectrum (400 MHz, DMSO-*d*$_6$) δ, ppm: 10.70 (s, 1H; NH), 10.06 (s, 1H; NH), 8.63 (d, *J*= 4.3 Hz, 2H; 3,5-bis(trifluoromethyl)phenyl), 8.44 (s, 2H; indole), 8.02 (d, *J*= 7.7 Hz, 1H; indole), 7.83 (s, 1H; 3,5-bis(trifluoromethyl)phenyl), 7.77 (d, *J*= 8.0 Hz, 1H; indole), 7.59 - 7.51 (m, 2H; Ar-F), 7.40 - 7.32 (m, 2H; indole), 7.12 (t, *J*= 8.9 Hz, 2H; Ar-F), 4.72 (t, *J*= 6.6 Hz, 2H; propanamide), 2.94 (t, *J*= 6.6 Hz, 2H; propanamide). Found %: C 59.14; H 3.24; N 9.50. $C_{29}H_{19}F_7N_4O_2$. Calculated, %: C 59.19; H 3.25; N 9.52. *M* 588.

(*Z*)-*N*-[3,5-bis(trifluoromethyl)phenyl]-3-(1-{3-[(4-chlorophenyl)amino]-3-oxo propyl}-1*H*-indol-3-yl)-2-cyanoacrylamide (9f)

Greenish yellow powder, Yield: 88%, mp 226-228 °C. IR spectrum, *v*, cm^{-1}: 1651 (C=O), 2198 (CN), 3279 (-NH-). ^{1}H NMR spectrum (400 MHz, DMSO-*d*$_6$) δ, ppm: 10.70 (s, 1H; NH), 10.14 (s, 1H; NH), 8.63 (d, *J*= 4.5 Hz, 2H; 3,5-bis(trifluoromethyl)phenyl), 8.44 (d, *J*= 1.6 Hz, 2H; indole), 8.03 (d, 1H; indole), 7.83 (s, 1H; 3,5-bis(trifluoromethyl)phenyl), 7.77 (d, *J*= 8.0 Hz, 1H; indole), 7.57 - 7.55 (m, 2H; Ar-Cl), 7.40 - 7.34 (m, 1H; indole), 7.38 - 7.31 (m, 2H; Ar-Cl+ indole), 7.32 (m, 1H; indole), 4.71 (t, *J*= 6.6 Hz, 2H; propanamide), 2.96 (t, *J*= 6.5 Hz, 2H; propanamide). Found %: C 57.59; H 3.17; N 9.28. $C_{29}H_{19}ClF_6N_4O_2$. Calculated, %: C 57.58; H 3.17; N 9.26. *M* 604.

(*Z*)-*N*-[3,5-bis(trifluoromethyl)phenyl]-2-cyano-3-(1-{3-[(2,6-dimethylphenyl) amino]-3-oxopropyl}-1*H*-indol-3-yl)acrylamide (9g)

Greenish yellow powder, Yield: 89%, mp 244-246 °C. IR spectrum, *v*, cm^{-1}: 1651 (C=O), 2198 (CN), 3263 (-NH-). ^{1}H NMR spectrum (400 MHz, DMSO-*d*$_6$) δ, ppm: 10.73 (s, 1H; NH), 9.31 (s, 1H; NH), 8.66 (d, 2H; 3,5-bis(trifluoromethyl)phenyl), 8.46 (s, 2H; indole),

8.04 (d, *J*= 7.6 Hz, 1H; indole), 7.83 (s, 1H; 3,5-bis(trifluoromethyl)phenyl), 7.78 (d, *J*= 7.9 Hz, 1H; indole), 7.41 - 7.33 (m, 2H; indole), 7.03 - 6.98 (m, 3H; xylidine), 4.73 (t, *J*= 6.3 Hz, 2H; propanamide), 2.98 (t, *J*= 6.3 Hz, 2H; propanamide), 1.93 (s, 6H; CH_3+CH_3). Found %: C, 62.19; H, 4.00; N, 9.32. $C_{31}H_{24}F_6N_4O_2$. Calculated, %: C 62.21; H 4.04; N 9.36. *M* 598.

(*Z*)-*N*-[3,5-bis(trifluoromethyl)phenyl]-2-cyano-3-(1-{3-[(2-fluorophenyl)amino]-3-oxopropyl}-1*H*-indol-3-yl)acrylamide (9h)

Greenish yellow powder, Yield: 78%, mp 220-222 °C. IR spectrum, *v*, cm^{-1}: 1666 (C=O), 2198 (CN), 3255 (-NH-). ^{1}H NMR spectrum (400 MHz, DMSO-d_6) δ, ppm: 10.70 (s, 1H; NH), 9.86 (s, 1H; NH), 8.63 (d, *J*= 6.9 Hz, 2H; 3,5-bis(trifluoromethyl)phenyl), 8.45 (s, 2H; indole), 8.02 (d, *J*= 7.7 Hz, 1H; indole), 7.88 (td, *J*= 7.6, 3.4 Hz, 1H; Ar-F), 7.81 (s, 1H; 3,5-bis(trifluoromethyl)phenyl), 7.76 (d, *J*= 8.0 Hz, 1H; indole), 7.40 - 7.32 (m, 2H; indole), 7.22 (ddd, *J*= 10.7, 6.7, 3.2 Hz, 1H; Ar-F), 7.14 (dq, *J*= 6.6, 3.8 Hz, 2H; Ar-F), 4.71 (t, *J*= 6.6 Hz, 2H; propanamide), 3.05 (t, *J*= 6.6 Hz, 2H; propanamide). Found %: C 59.15; H 3.22; N 9.50. $C_{29}H_{19}F_7N_4O_2$. Calculated, %: C 59.19; H 3.25; N 9.52. *M* 588.

(*Z*)-*N*-[3,5-bis(trifluoromethyl)phenyl]-2-cyano-3-{1-[3-oxo-3-(*o*-tolylamino)propyl]-1*H*-indol-3-yl}acrylamide (9i)

Greenish yellow powder, Yield: 84%, mp 208-210 °C. IR spectrum, *v*, cm^{-1}: 1643 (C=O), 2198 (CN), 3279 (-NH-). ^{1}H NMR spectrum (400 MHz, DMSO-d_6) δ, ppm: 10.72 (s, 1H; NH), 9.39 (s, 1H; NH), 8.64 (d, *J*= 9.6 Hz, 2H; 3,5-bis(trifluoromethyl)phenyl), 8.46 (s, 2H; indole), 8.04 - 8.02 (d, 1H; indole), 7.82 (s, 1H; 3,5-bis(trifluoromethyl)phenyl), 7.77 (d, *J*= 8.0 Hz, 1H; indole), 7.41 - 7.29 (m, 3H; indole+ toluidine), 7.16 - 7.10 (m, 2H; indole+ toluidine), 7.05 (td, *J*= 7.4, 1.4 Hz, 1H; toluidine), 4.73 (t, *J*= 6.5 Hz, 2H; propanamide), 2.98 (t, *J*= 6.5 Hz, 2H; propanamide), 2.03 (s, 3H; CH_3). Found %: C 61.68; H 3.82; N 9.61. $C_{30}H_{22}F_6N_4O_2$. Calculated, %: C 61.65; H 3.79; N 9.59. *M* 584.

(*Z*)-*N*-[3,5-bis(trifluoromethyl)phenyl]-2-cyano-3-{1-[3-oxo-3-(*p*-tolylamino)propyl]-1*H*-indol-3-yl}acrylamide (9j)

Greenish yellow powder, Yield: 83%, mp 227-229 °C. IR spectrum, *v*, cm^{-1}: 1643 (C=O), 2198 (CN), 3286 (-NH-). ^{1}H NMR spectrum (400 MHz, DMSO-d_6) δ, ppm: 10.70 (s, 1H; NH), 9.91 (s, 1H; NH), 8.63 (d, *J*= 3.0 Hz, 2H; 3,5-bis(trifluoromethyl)phenyl), 8.44 (s, 2H; indole), 8.02 (d, *J*= 7.7 Hz, 1H; indole), 7.83 (s, 1H; 3,5-bis(trifluoromethyl)phenyl),

7.77 (d, *J*= 8.0 Hz, 1H; indole), 7.45 - 7.35 (m, 3H; toluidine+ indole), 7.35 - 7.32 (m, 1H; indole), 7.08 (d, *J*= 8.3 Hz, 2H; toluidine), 4.71 (t, *J*= 6.6 Hz, 2H; propanamide), 2.93 (t, *J*= 6.6 Hz, 2H; propanamide), 2.23 (s, 3H; CH_3). Found %: C 61.68; H 3.82; N 9.61. $C_{30}H_{22}F_6N_4O_2$. Calculated, %: C 61.65; H 3.79; N 9.59. *M* 584.

2.3.2 Malaria inhibitor prediction

The indole-based compound library was analyzed for a computational method which is a web service for predicting blood stage malaria inhibitor (MAIP) using QSAR model. Each compound was passed through standardization procedure and generate the score which indicate the compound with higher score is active at given threshold against blood stage malaria. The model was developed using the Naïve Bayes model. The training of the dataset was done by the eleven different dataset which consist of Evotec, Johns Hopkins, MRCT, AZ, GSK, St. Jude Vendor Library dataset, Novartis and MMV -St. Jude. The three additional datasets were provided by the Medicines for Malaria Venture (MMV) which includes MMV_5, MMV_6, and MMV_7 dataset. The model validation was achieved by three different dataset which contains MMV test set, the PubChem data set and ST. Jude screening set.[155] It is complex to deal with different eleven dataset in respective of system performance therefor a web application which is a metamodel known as MAIP (MAlaria Inhibitor prediction) is accessible at https://www.ebi.ac.uk/chembl/maip/ . The library containing thirty-five indole-based scaffolds was converted to smile strings using MarvinSketch software and a csv file was prepared in MS excel containing smile strings which was submitted at web application. After completion of the task a file containing discrete score of compounds and standardized compound structure can be obtained from web application.

2.3.3 *In vitro* antimalarial activity

The *in vitro* antimalarial activity was carried out by following the micro assay protocol by rieckmann *et. al* in 96 well microtiter plates with some modifications.[156] The cultures consisting 3D7 strain of Plasmodium falciparum were supplemented with 25 mM HEPES, 1% D-glucose, 0.23% sodium bicarbonate and 10% heat inactivated human serum and maintained in medium RPMI 1640. To derive only the ring stage parasitized cells the asynchronous parasite of P. falciparum was synchronized after giving treatment with 5% D-sorbitol.[157] To perform activity, the primary ring stage parasitaemia of 0.8 to 1.5% at 3%

haematocrit in a total volume of 200 µl of medium RPMI-1640 was resolved by JSB staining to evaluate the percent parasitaemia(rings) and uniformly maintained with 50% RBCs(O^+).[158] Each of the test samples were produce in DMSO with a stock solution of 5 mg/ml and further dilutions were made with culture medium. In order to achieve final concentrations (at fivefold dilutions) ranging from 0.4 g/ml to 100 g/ml in duplicate wells containing parasitized cell preparation, the diluted samples in 20 µl volume were introduced to the test wells.[159] The candle jar was used for the incubation of culture plates at 37°C and after 36 to 40h of incubation, from each well thin blood smears were prepared and stained by the JSB method.[160] The maturations of the ring stage parasites into trophozoites and schizonts in presence of varied concentrations of the test agents the slides were observed microscopically. The minimal inhibitory concentration was determined to be the test concentration that completely inhibited the development into schizonts (MIC).[161] The chloroquine was used as a standard drug. after 38 hours of incubation, the average number of rings, trophozoites, and schizonts per 100 parasites was counted from duplicate wells, along with the percentage of maturation inhibition compared to the control group.

2.3.4 *In silico* activity against PfDHFR

Molecular docking studies were performed using PyRX 0.8, which utilizes the AutoDock Vina (1.1.2) software for the docking analysis.[162] The goal of the study was to find the binding interactions between the target protein (PDB id: 3QGT) and a series of ligands, including the standard drug chloroquine and ten synthesized compounds **9a-j**, in order to assess their potential as inhibitors.

- **Target Protein:** The Protein Data Bank (PDB) was used to obtain the target protein 3QGT's crystal structure. The protein structure was prepared by removing water molecules and the co-crystallized ligands. Hydrogen atoms were added, and charges were assigned using the amber force field.
- **Ligands:** The ligands used in this study include chloroquine and ten synthesized compounds, **9a-j**. Chloroquine was obtained commercially, while the synthesized compounds were prepared in the laboratory according to the method mentioned above and the structure were prepared for docking in Chemsketch 2022.2.3. The

ligand structures were optimized for geometry and charges using Open Babel software (3.1.1) with UFF forcefield.[163]

- **Docking Setup:** The docking grid was defined based on the presumed binding site of the target protein (3QGT). The specific binding site was identified through analysis of the protein structure and relevant literature.[164] The grid parameters were set to accommodate ligand flexibility and to allow for possible ligand conformations during the docking process. The grid center coordinates were set as 28.60, 9.57, 58.00, and the grid size was defined as 19.18, 29.91, 19.56. Exhaustiveness and other relevant parameters were set to default values, as recommended by the AutoDock Vina guidelines.[165]
- **Docking Analysis:** The ligands, including chloroquine and the synthesized compounds **9a-j**, were docked at the active site of the target protein (3QGT) using AutoDock Vina in PyRX. Multiple docking runs were performed, and the output poses were ranked based on their binding energies. The docking results were analyzed using Discovery Studio Visualizer (2021) to examine ligand-protein interactions, hydrogen bonding, and hydrophobic interactions.

2.4 Conclusion

In summary the novel series of indole derivatives were designed and screened for active derivatives against plasmodium falciparum. These active compounds **9a-j** were synthesized and characterized by various spectroscopic methods namely ^{1}H NMR, Mass spectroscopy and FT-IR. The *in vitro* antimalarial activity was performed against Plasmodium falciparum and result manifested different activity levels of the synthesized compounds. For the further findings to evaluate the potential efficacy of the compounds **9a-j** the molecular modeling was performed against PfDHFR enzyme of plasmodium falciparum analyzing possible mechanism of action. These findings indicated that the synthesized compounds **9a-j** are highly active towards PfDHFR binding sites. All the compounds have shown least binding energy than the standard drug chloroquine among which compound **9g** has lowest binding energy of -11.1 while chloroquine has -7.1. The trifluoromethyl group also shows the good interaction by halogen bonding with various

amino acids. The findings of this research will helpful in providing further optimization and development of selective agents which are more potent for malaria.

2.5 Spectral data

- **Spectral data of compound 9a**

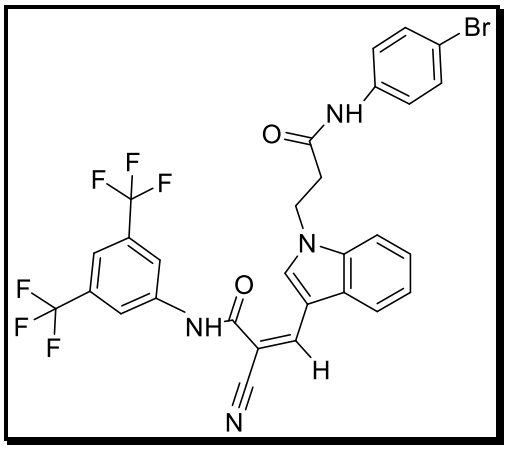

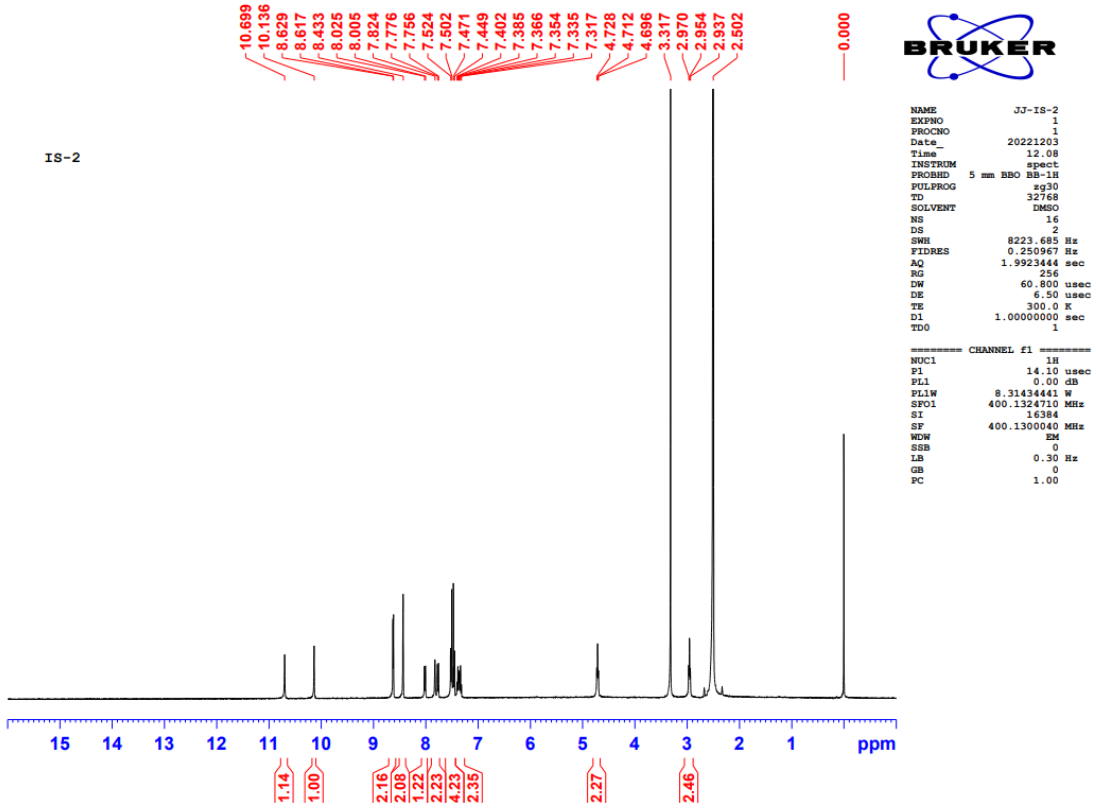

Figure 9: Representative ^{1}H NMR spectrum of compound 9a

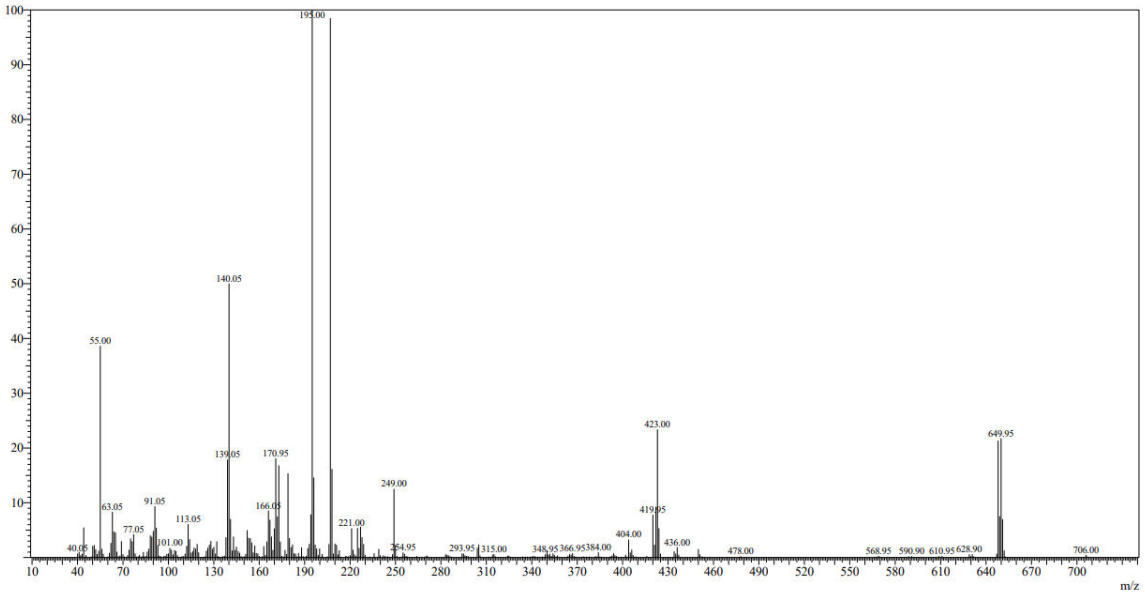

Figure 10: Representative mass spectrum of compound 9a

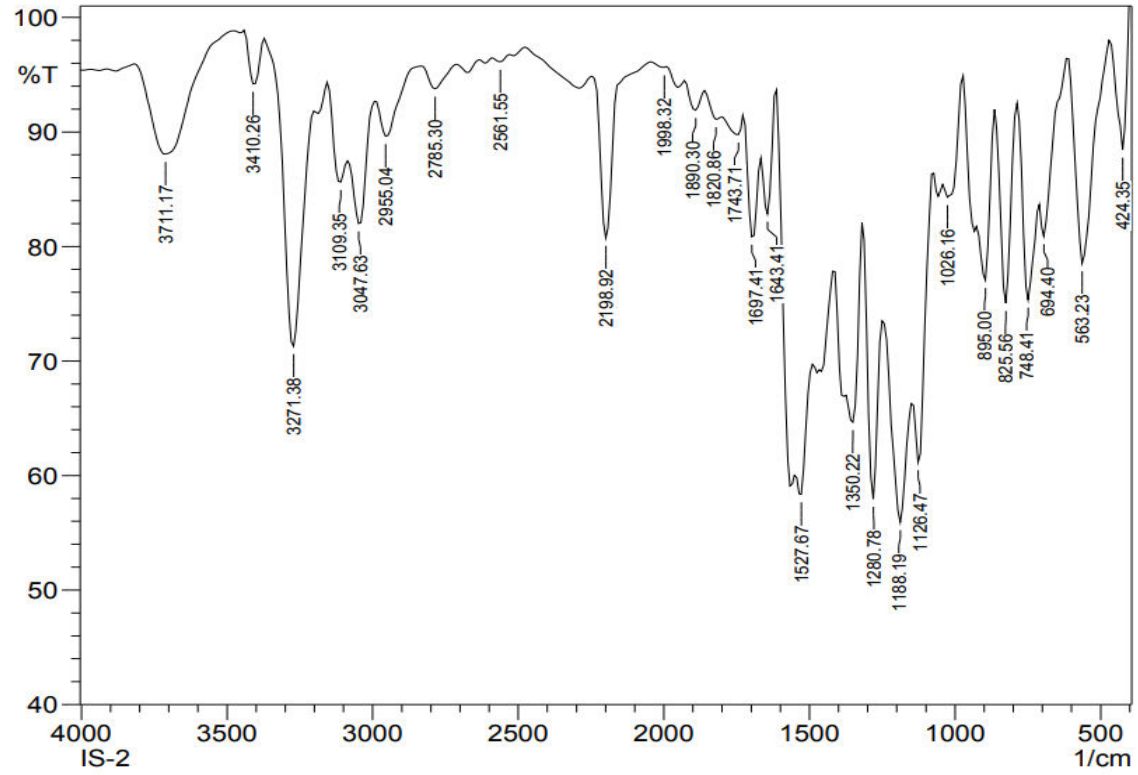

Figure 11: Representative FT-IR spectrum of compound 9a

- **Spectral data of compound 9b**

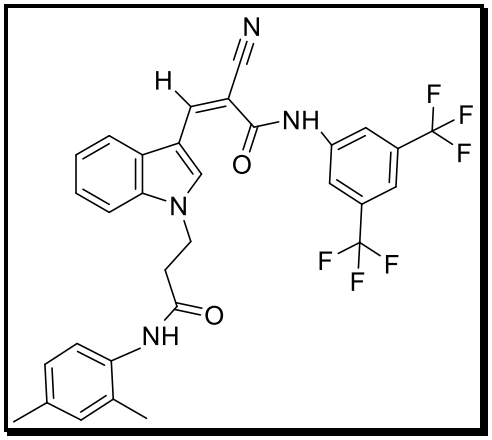

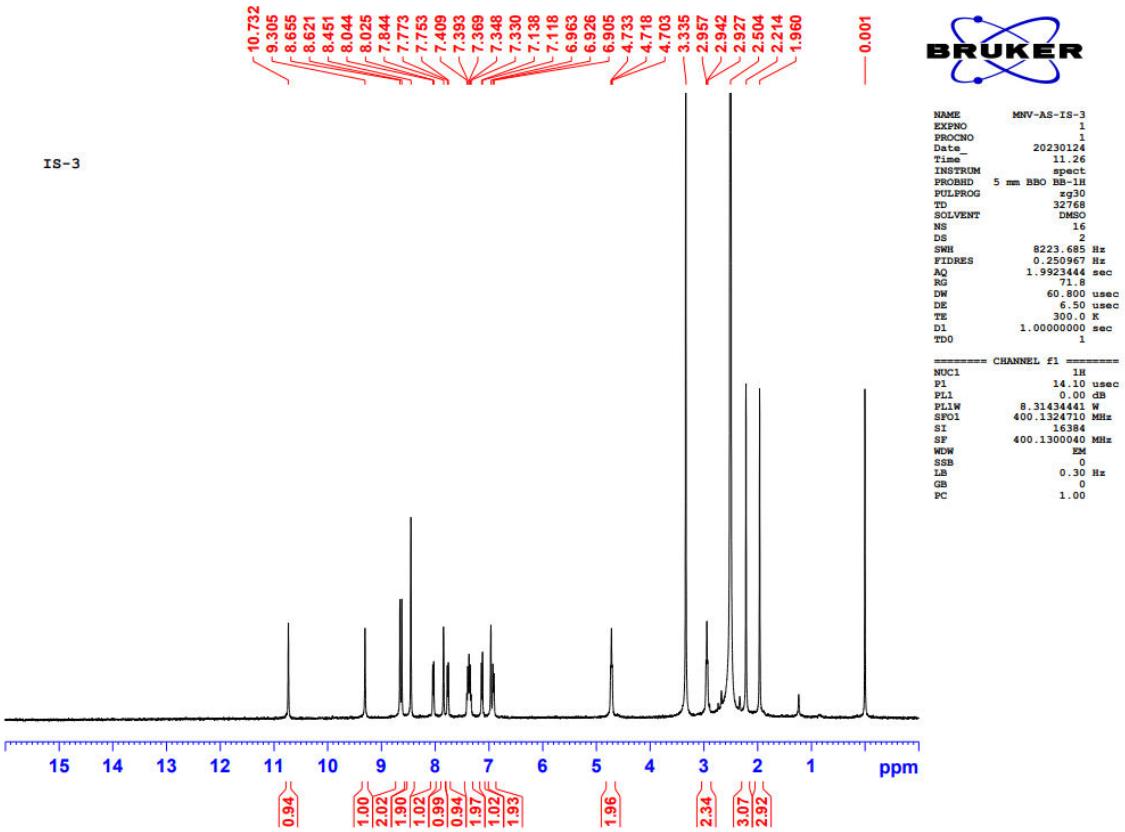

Figure 12: Representative ^{1}H NMR spectrum of compound 9b

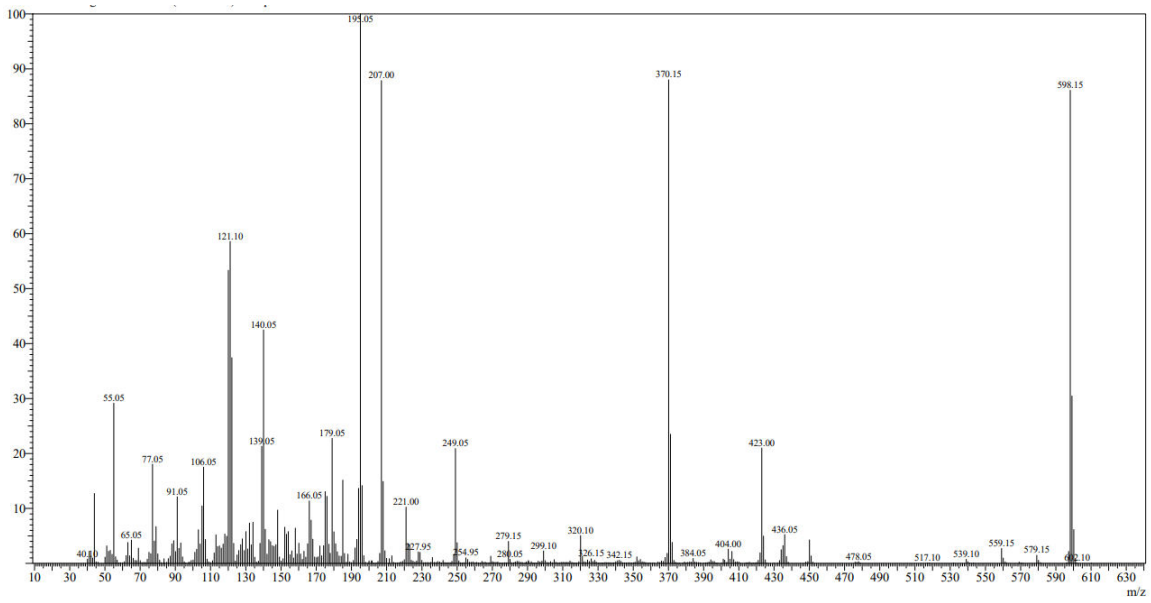

Figure 13: Representative mass spectrum of compound 9b

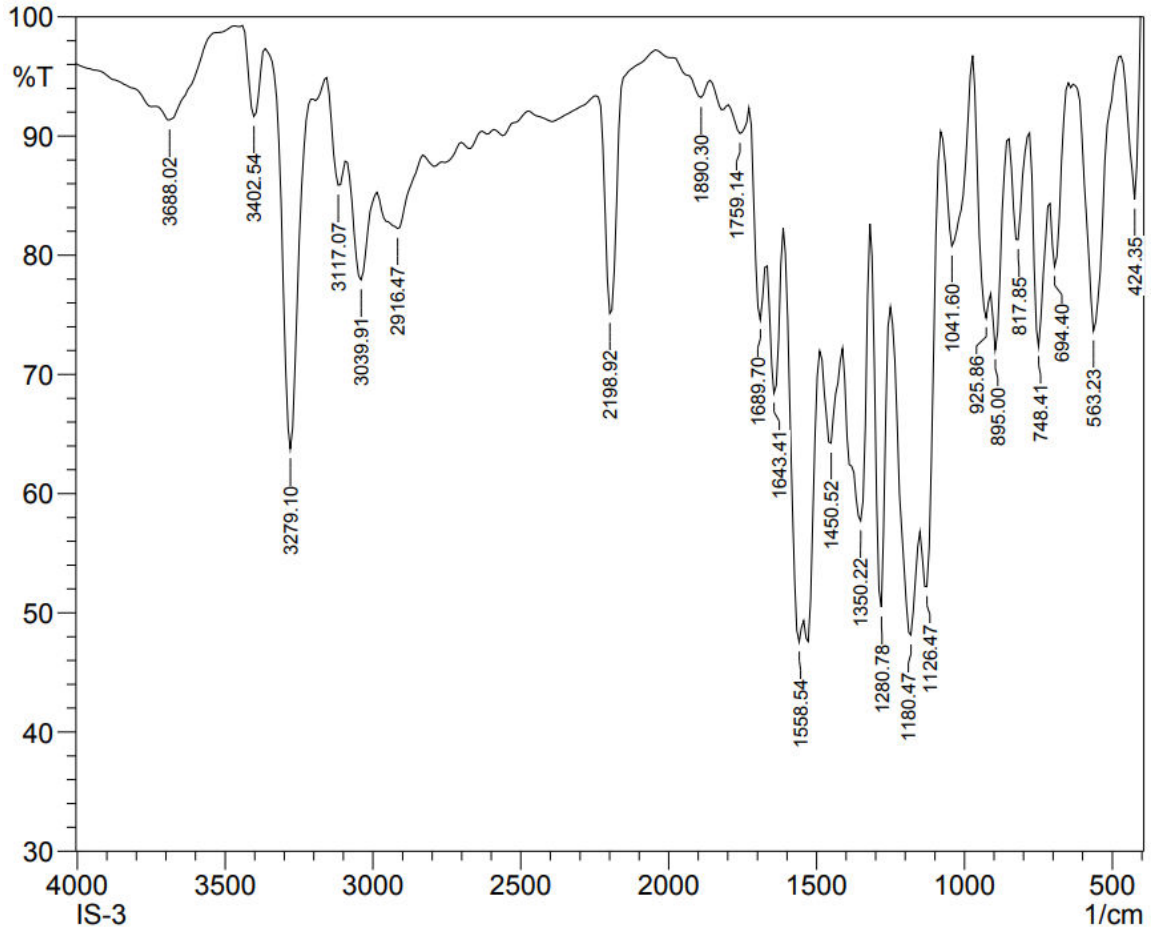

Figure 14: Representative FT-IR spectrum of compound 9b

- **Spectral data of compound 9c**

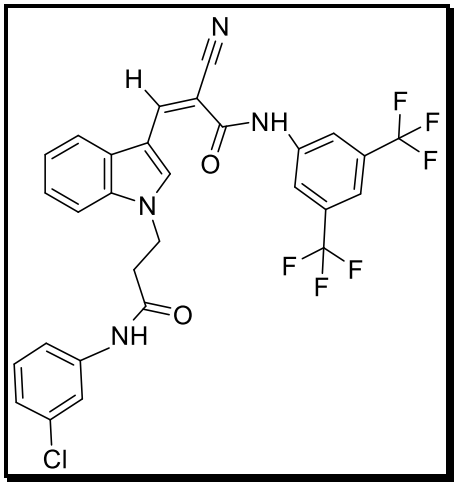

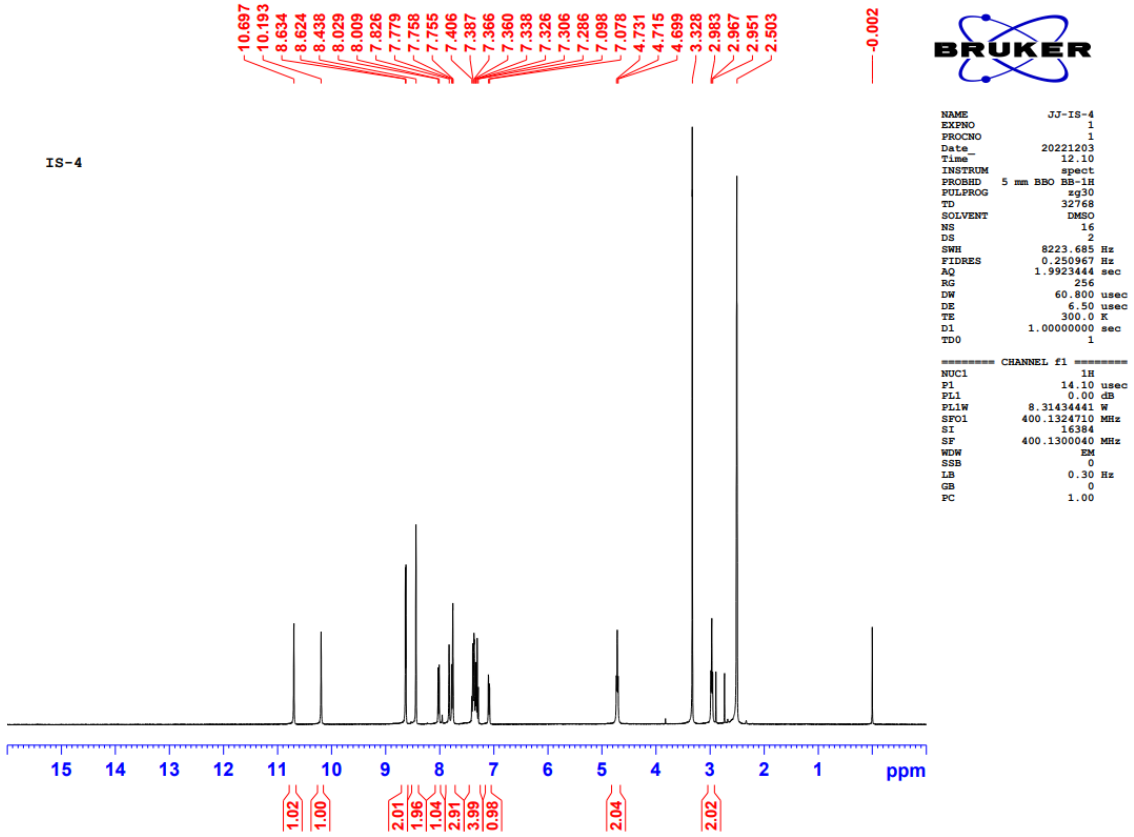

Figure 15: Representative ^{1}H NMR spectrum of compound 9c

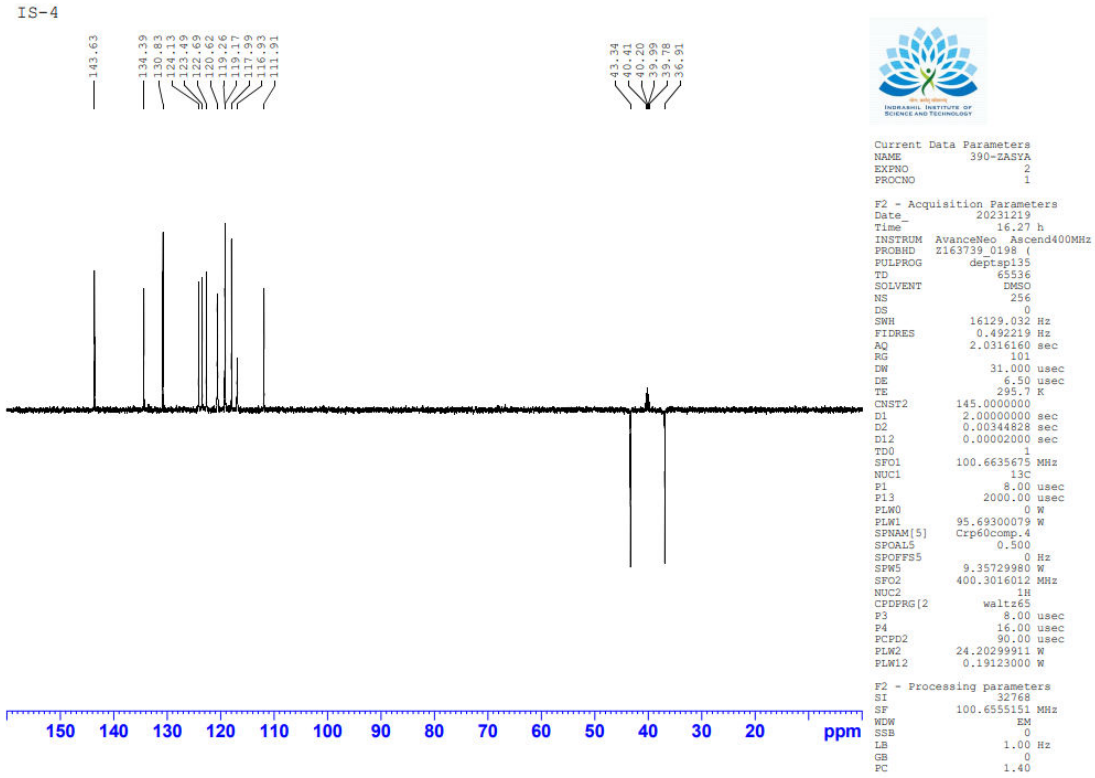

Figure 16: Representative ^{13}C DEPT-135 NMR of compound 9c

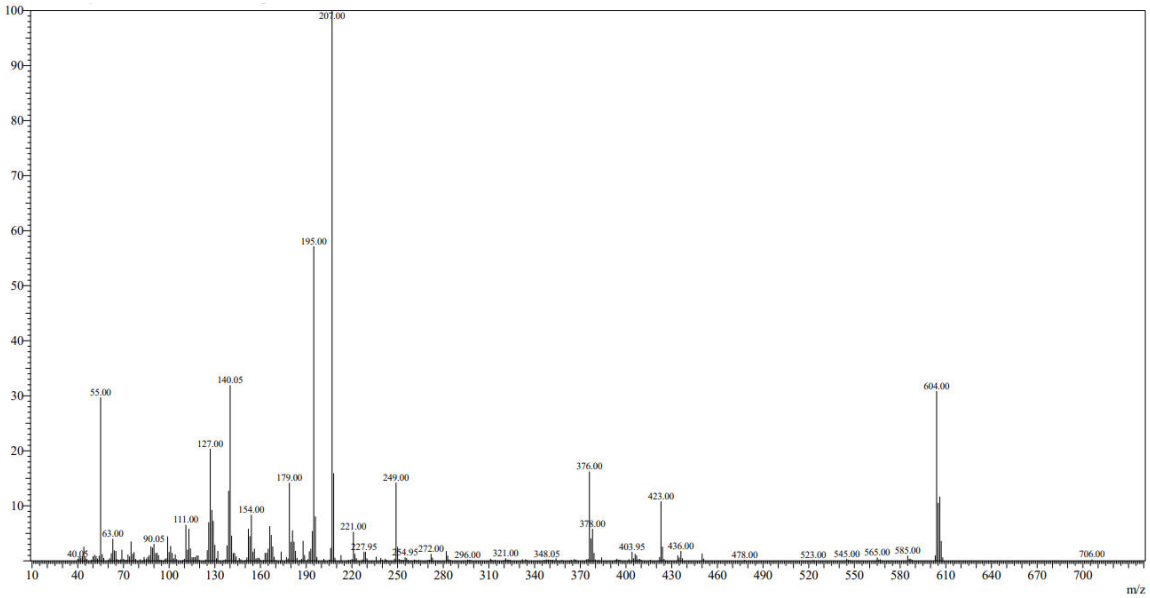

Figure 17: Representative mass spectrum of compound 9c

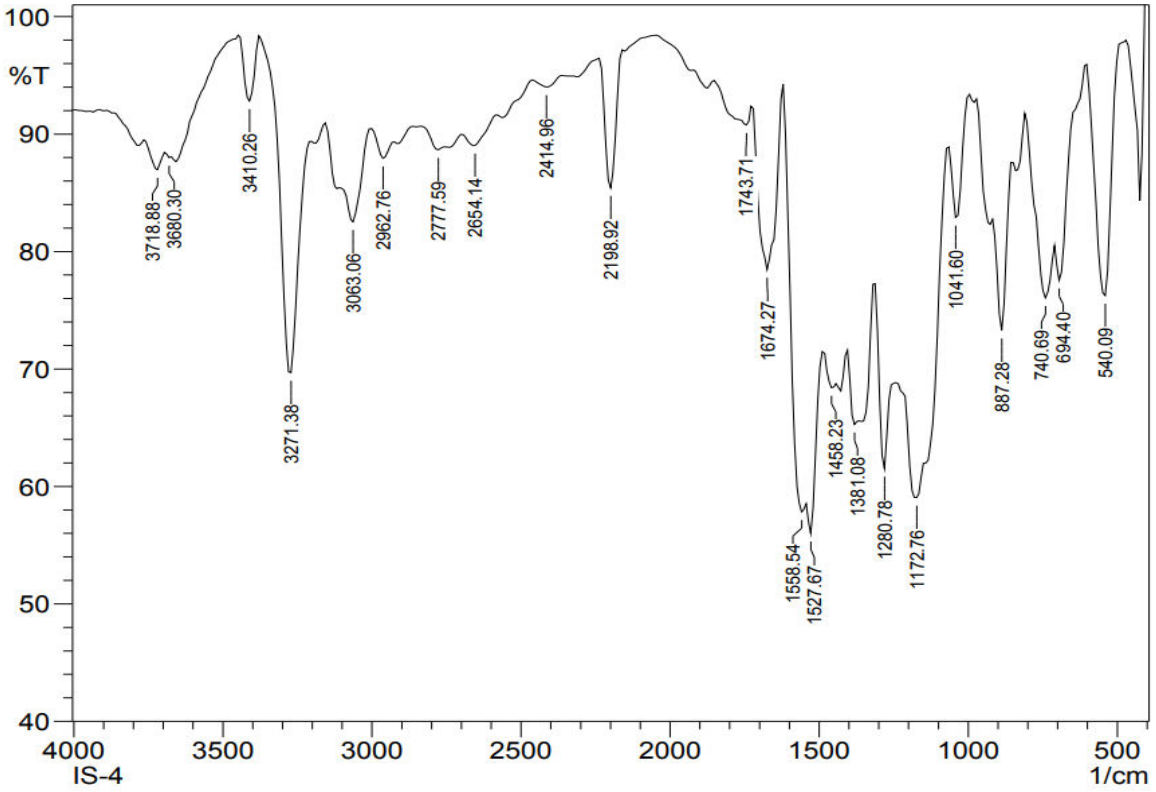

Figure 18: Representative FT-IR spectrum of compound 9c

- **Spectral data of compound 9d**

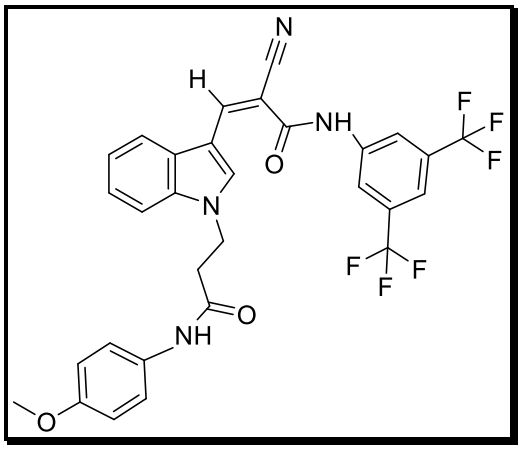

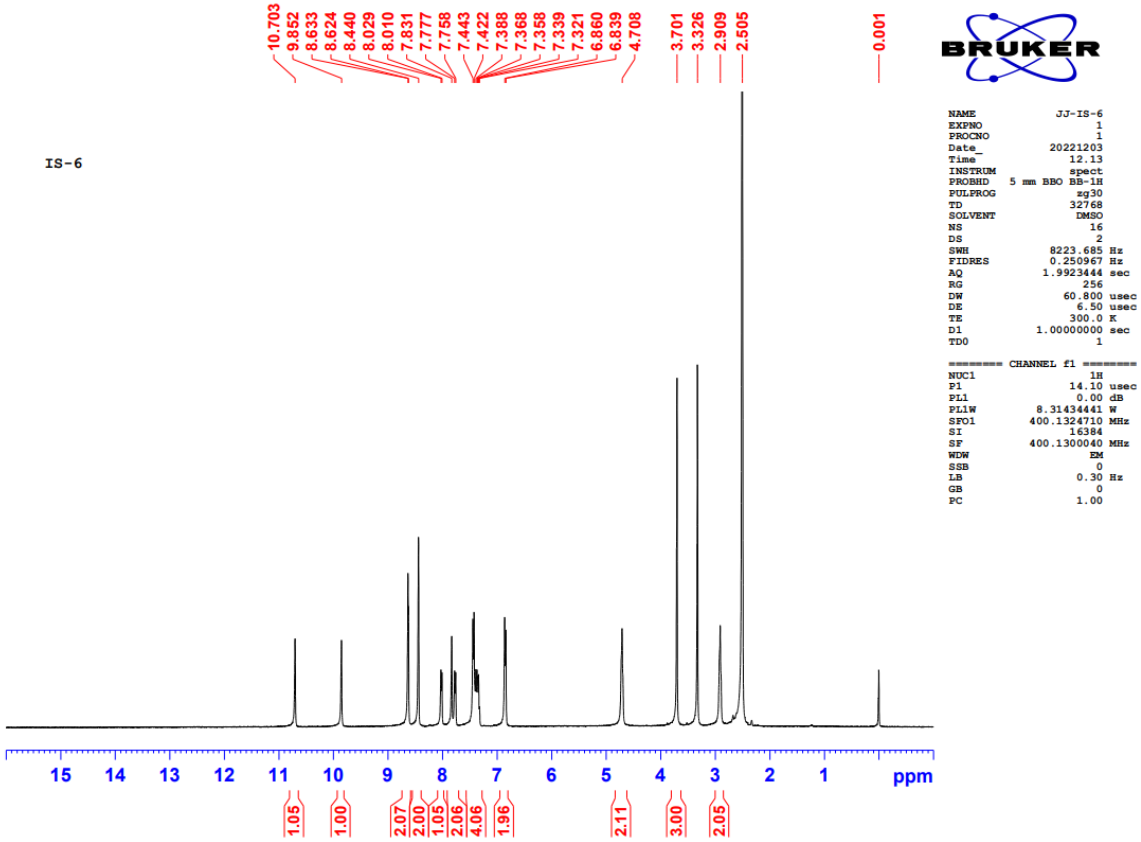

Figure 19: Representative ^{1}H NMR spectrum of compound 9d

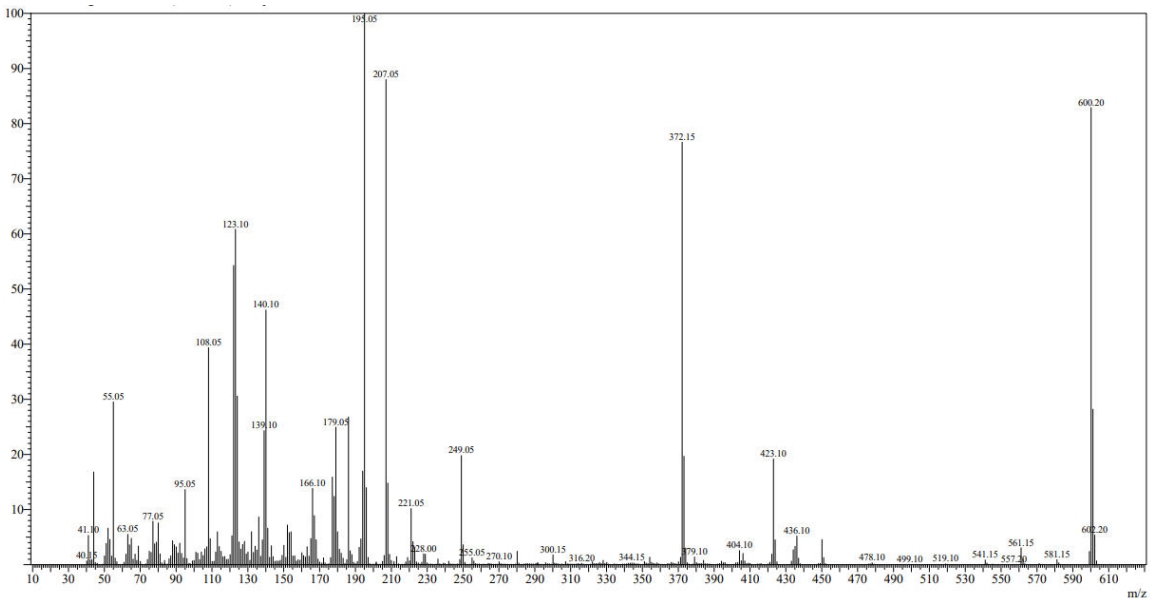

Figure 20: Representative mass spectrum of compound 9d

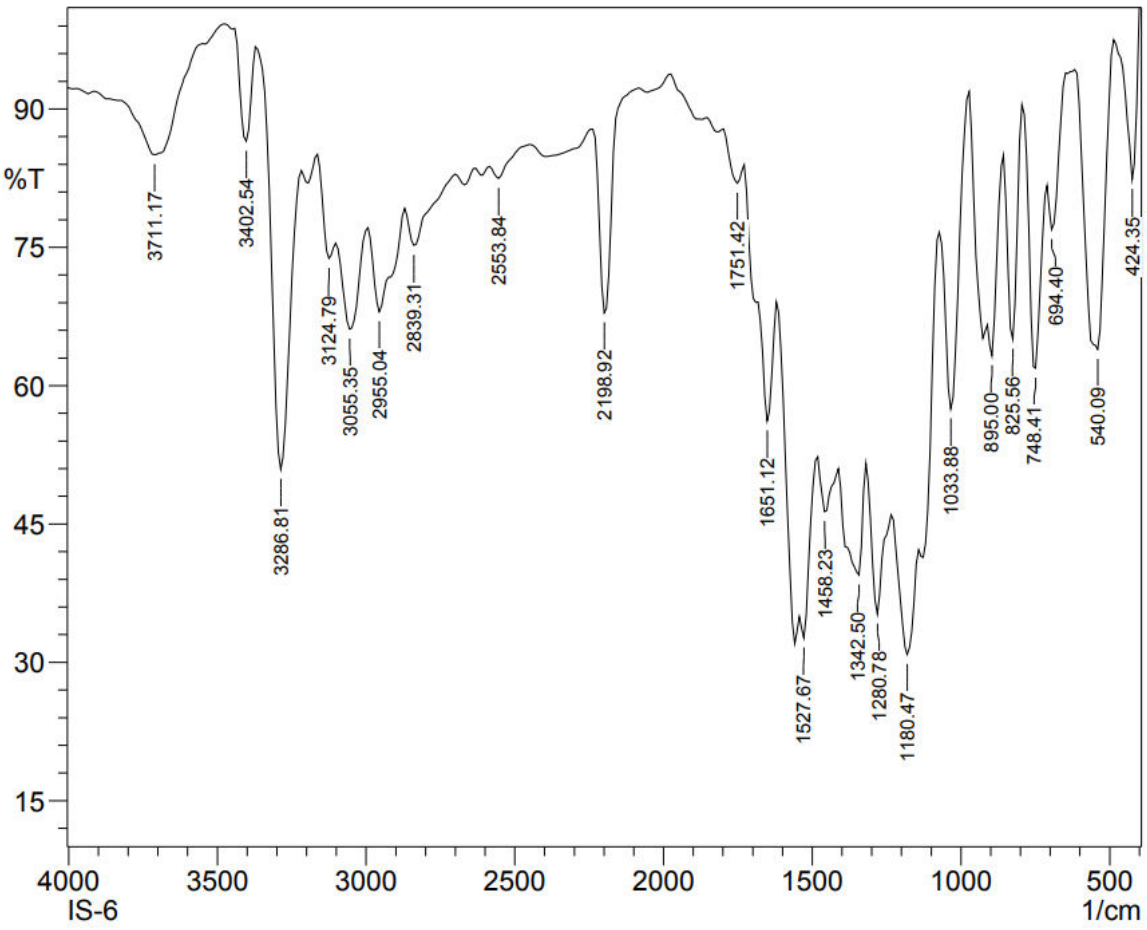

Figure 21: Representative FT-IR spectrum of compound 9d

- **Spectral data of compound 9e**

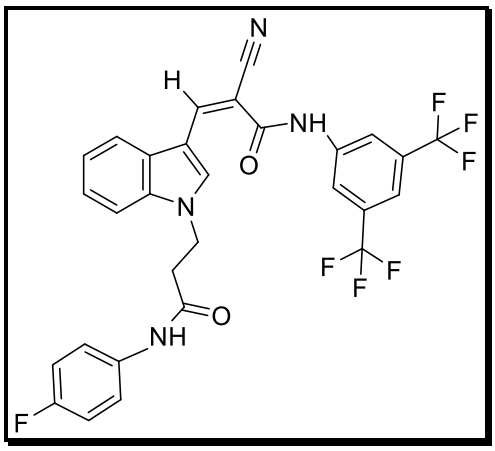

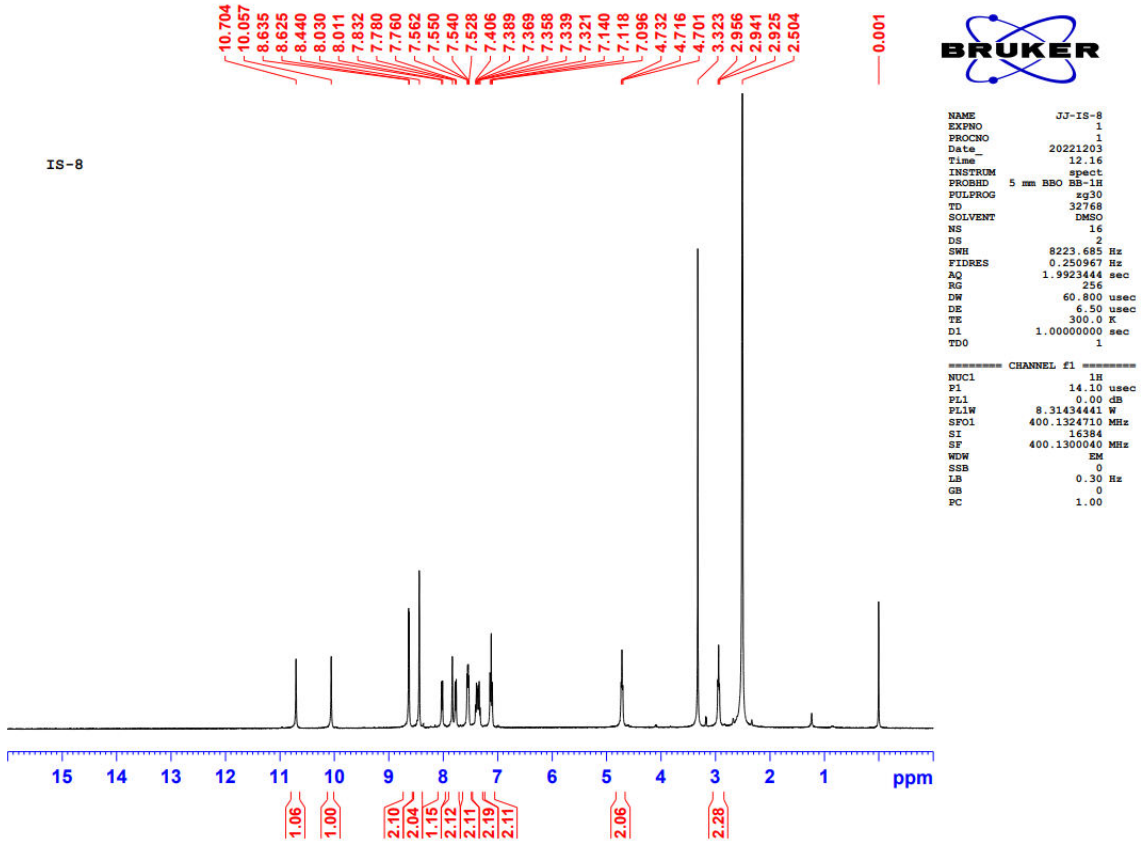

Figure 22: Representative ^{1}H NMR spectrum of compound 9e

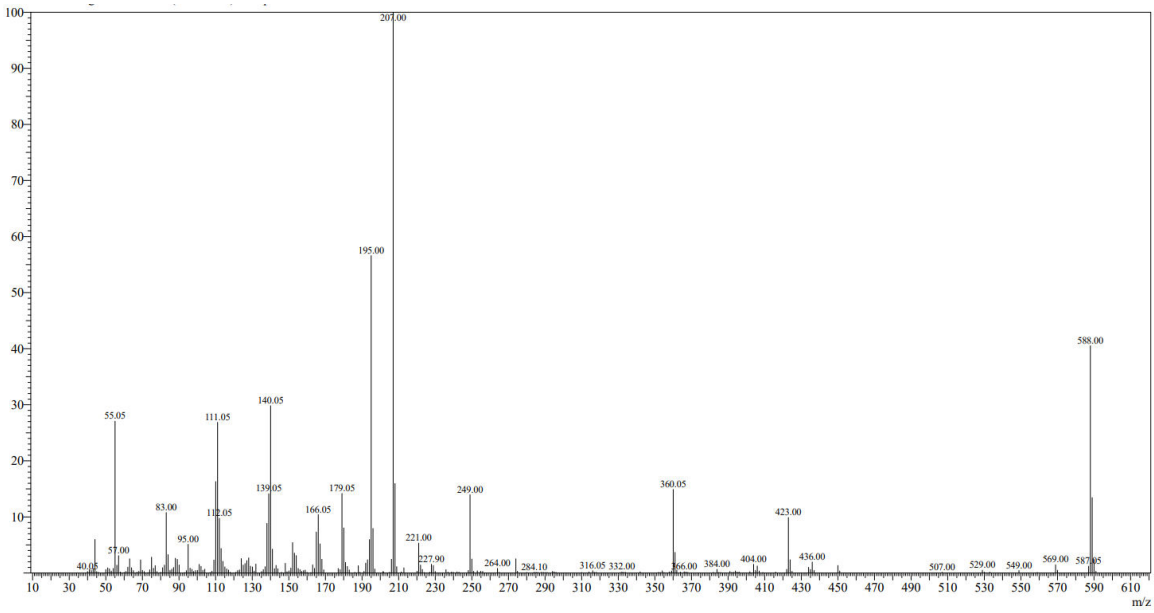

Figure 23: Representative mass spectrum of compound 9e

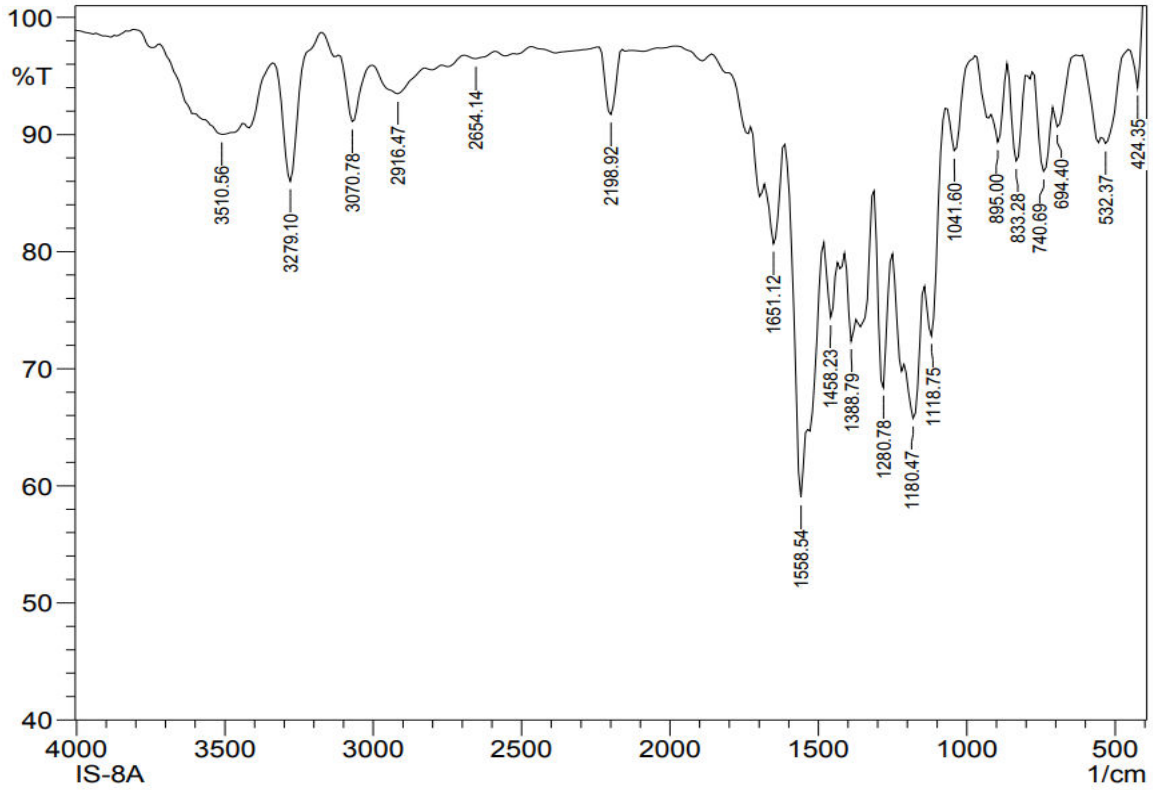

Figure 24: Representative FT-IR spectrum of compound 9e

- **Spectral data of compound 9f**

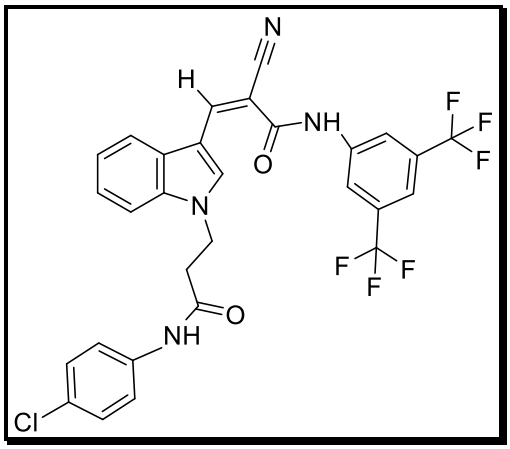

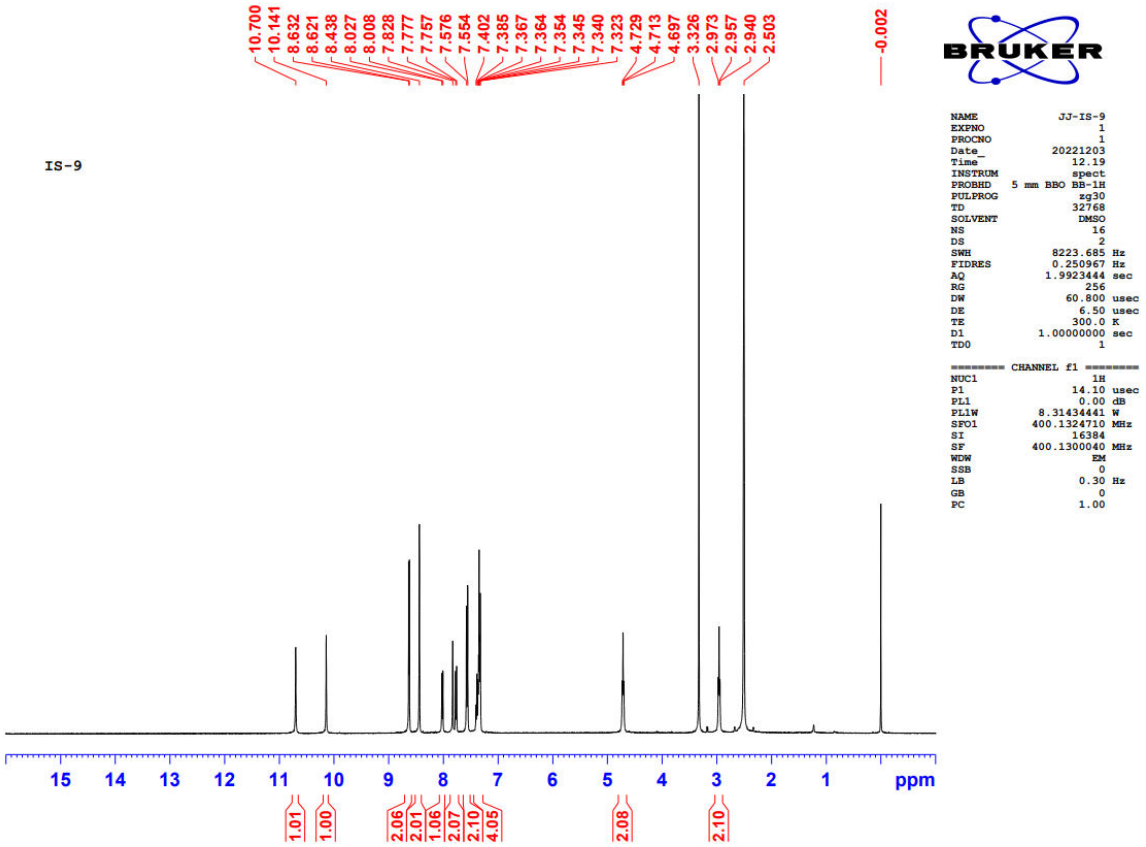

Figure 25: Representative ^{1}H NMR spectrum of compound 9f

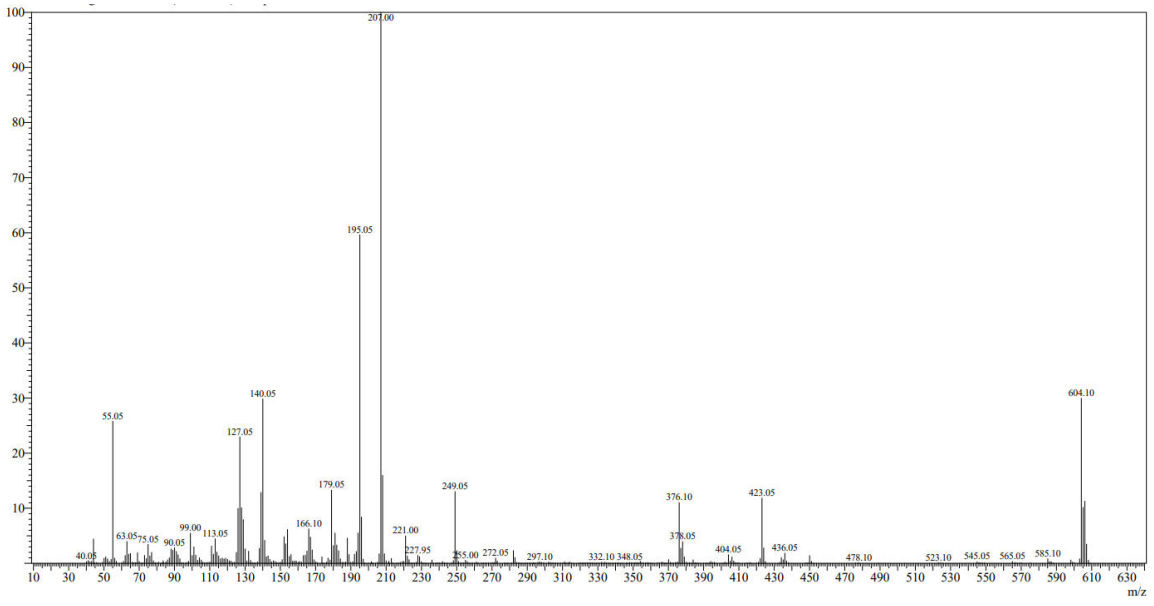

Figure 26: Representative mass spectrum of compound 9f

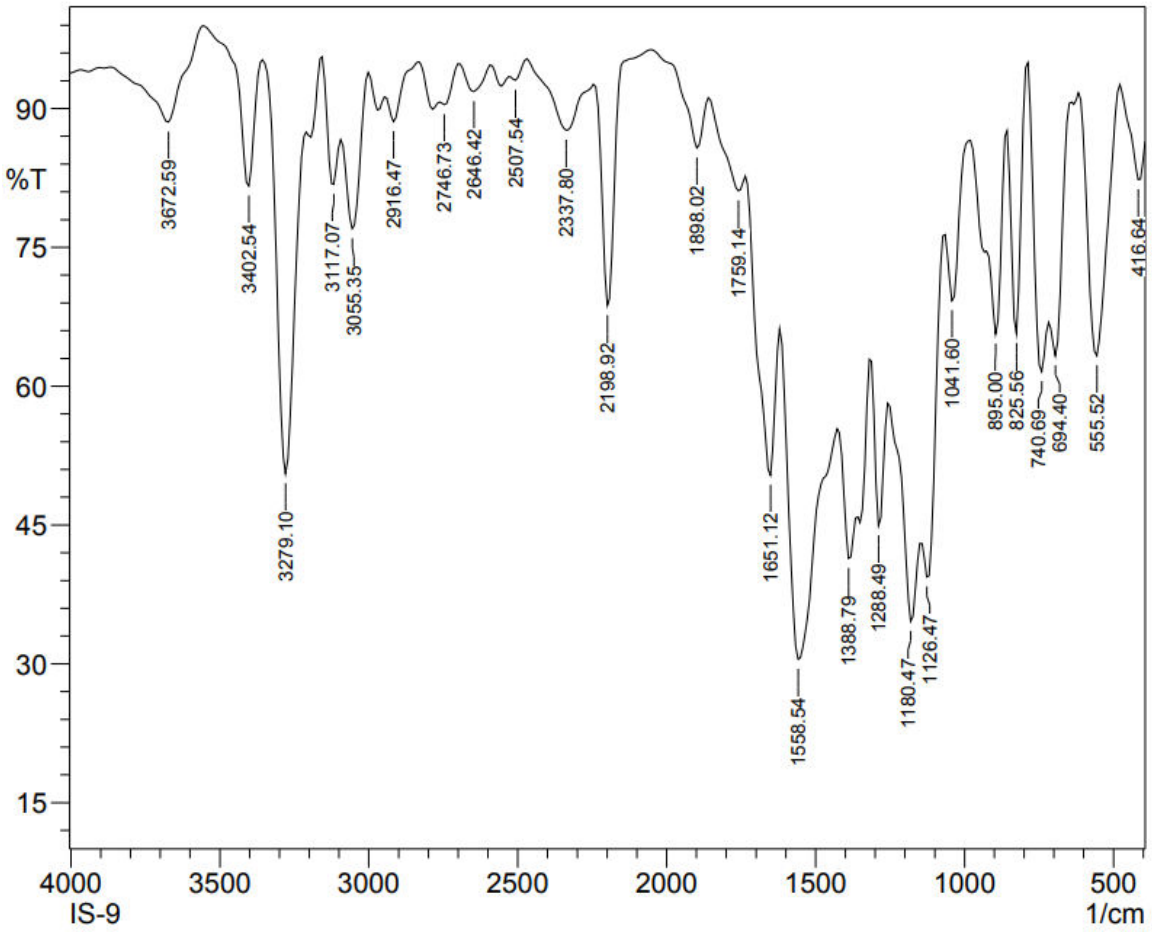

Figure 27: Representative FT-IR spectrum of compound 9f

- **Spectral data of compound 9g**

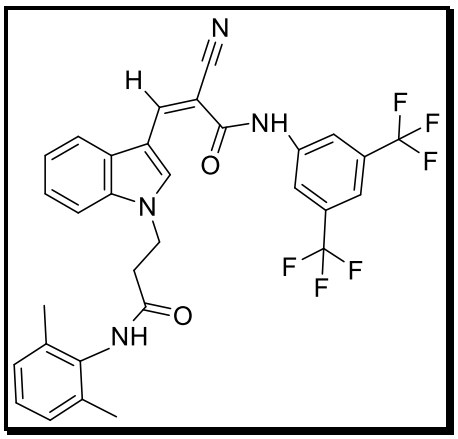

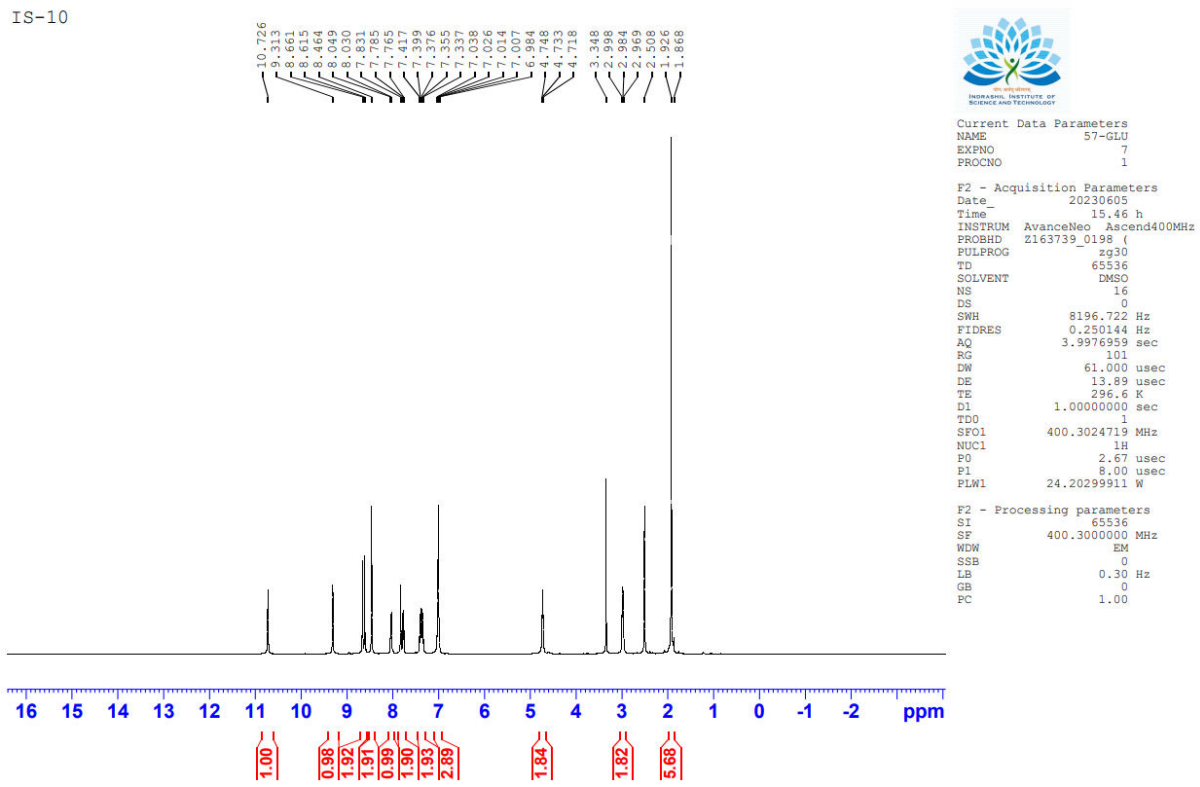

Figure 28: Representative ^{1}H NMR spectrum of compound 9g

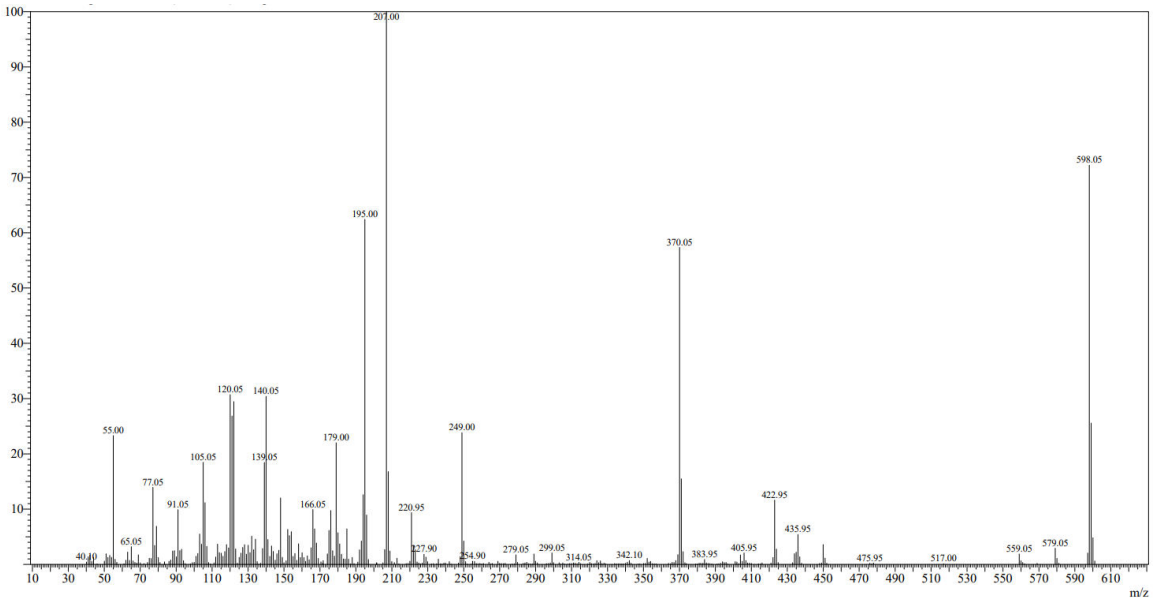

Figure 29: Representative mass spectrum of compound 9g

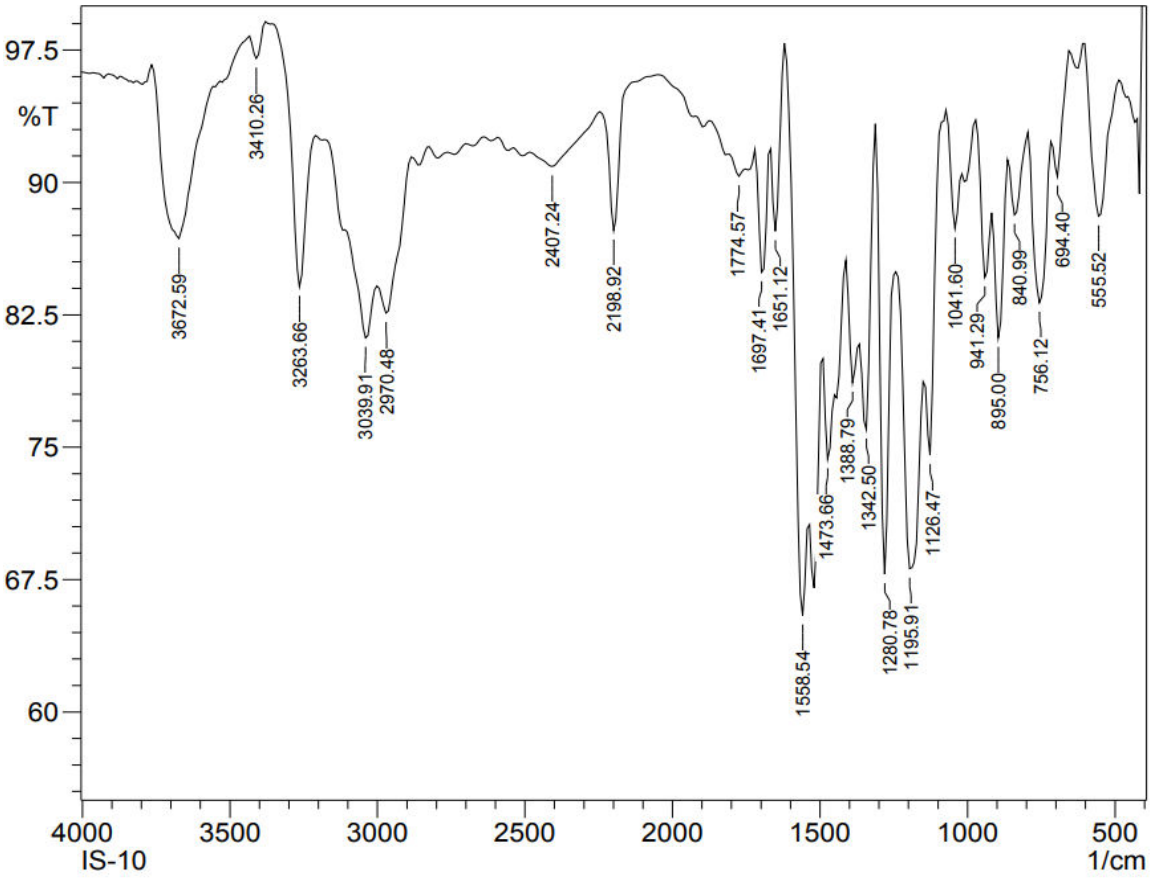

Figure 30: Representative FT-IR spectrum of compound 9g

- **Spectral data of compound 9h**

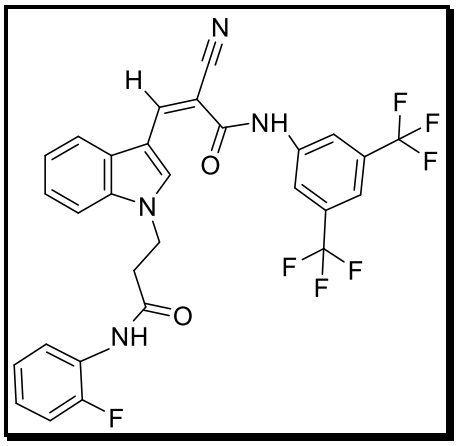

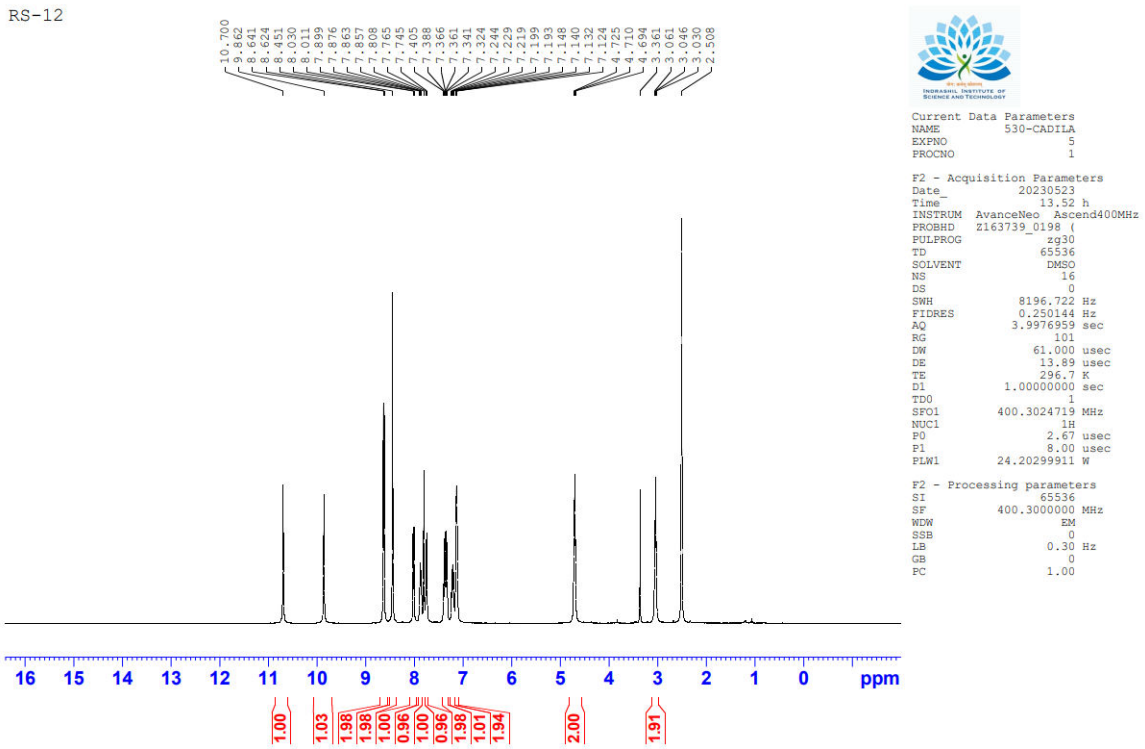

Figure 31: Representative ^{1}H NMR spectrum of compound 9h

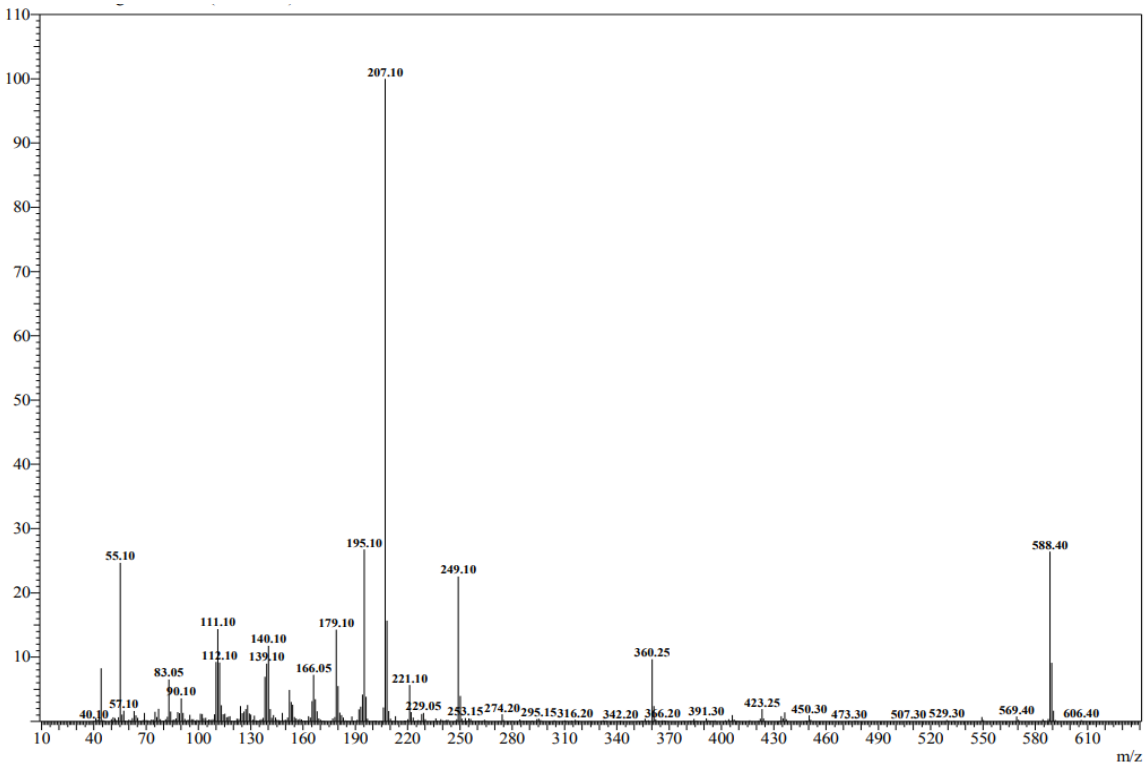

Figure 32: Representative mass spectrum of compound 9h

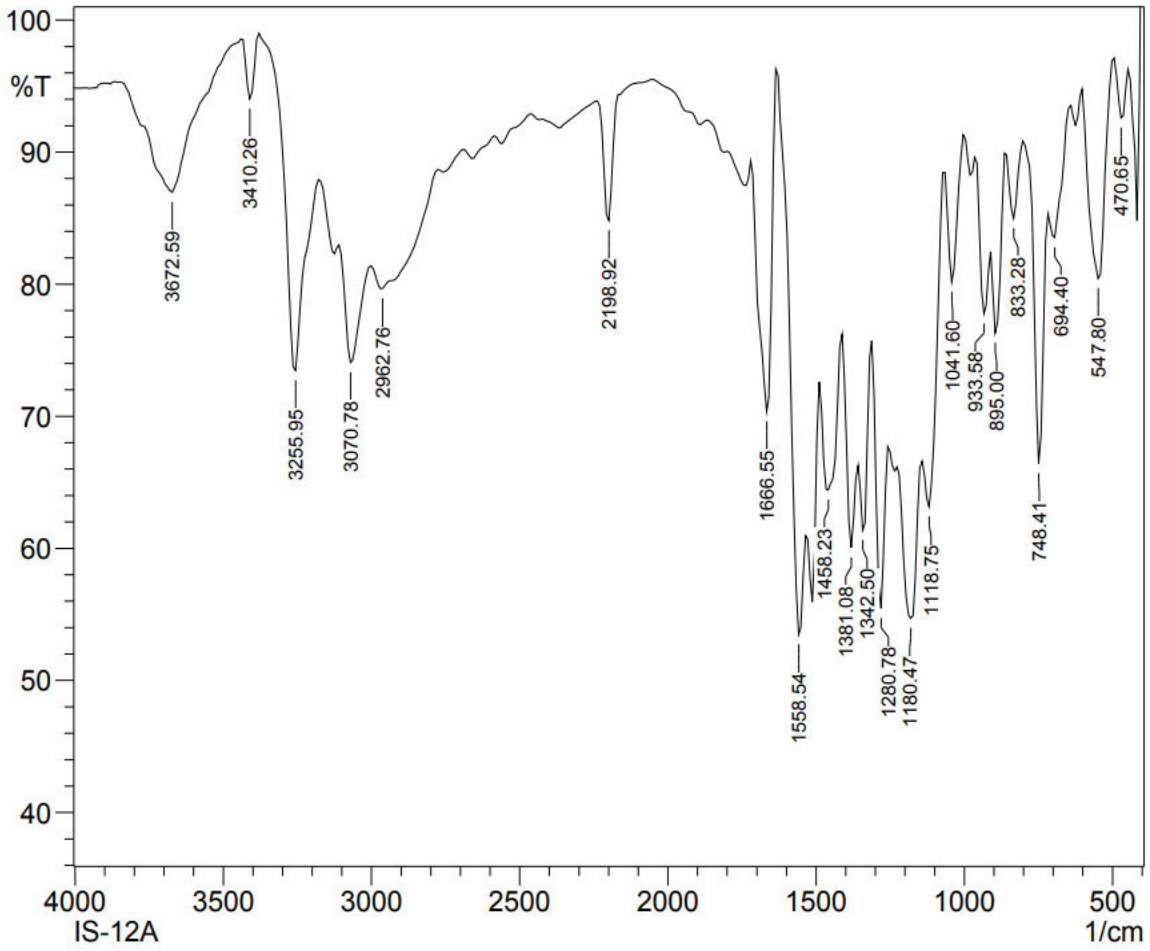

Figure 33: Representative FT-IR spectrum of compound 9h

- **Spectral data of compound 9i**

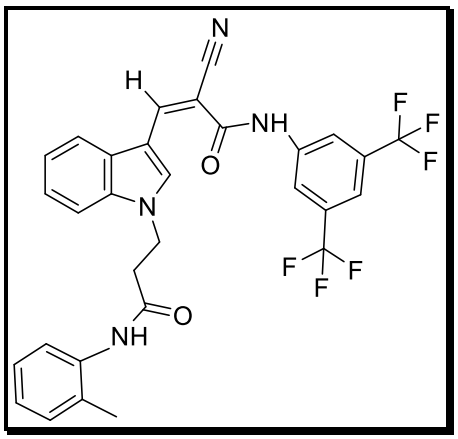

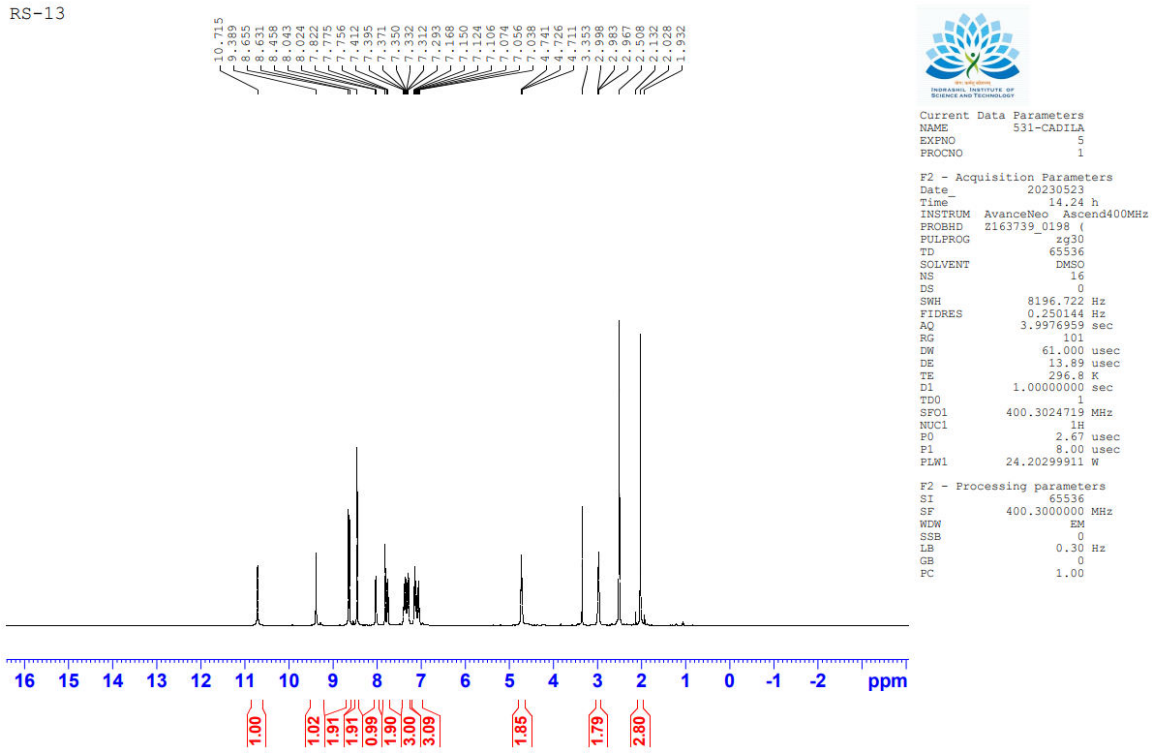

Figure 34: Representative ^{1}H NMR spectrum of compound 9i

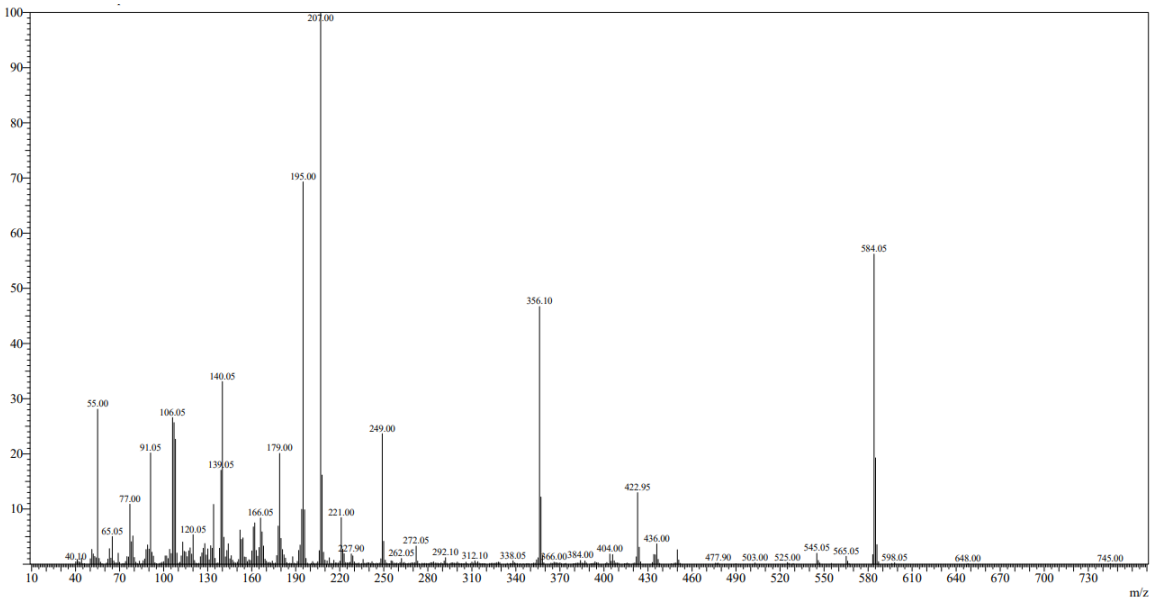

Figure 35: Representative mass spectrum of compound 9i

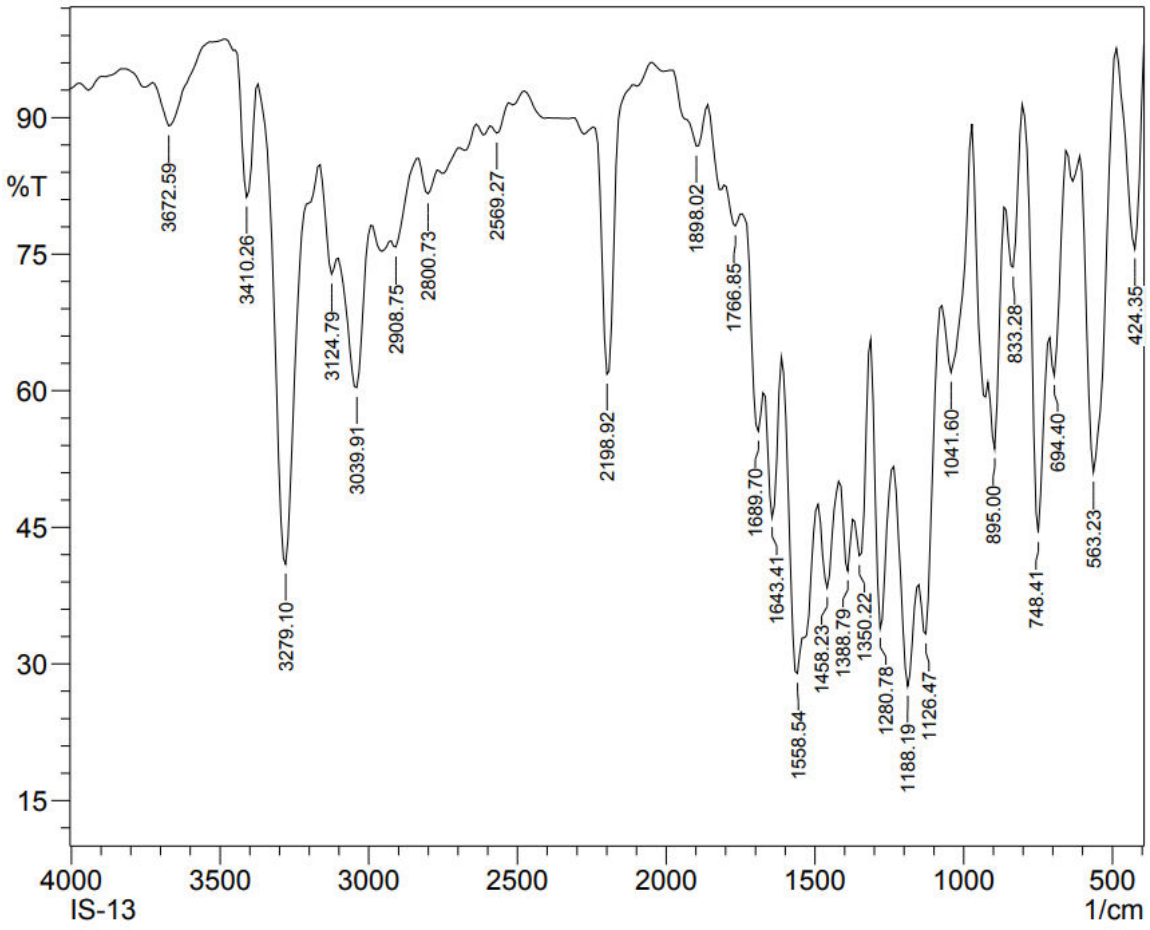

Figure 36: Representative FT-IR spectrum of compound 9i

- **Spectral data of compound 9j**

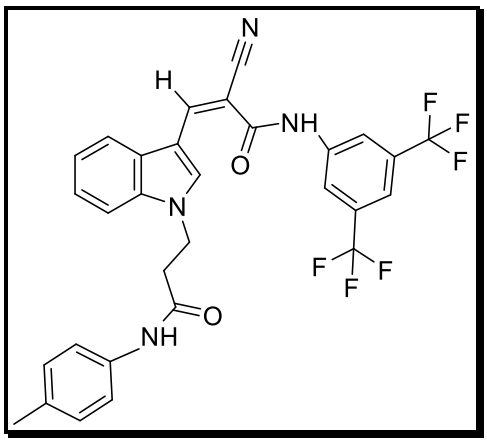

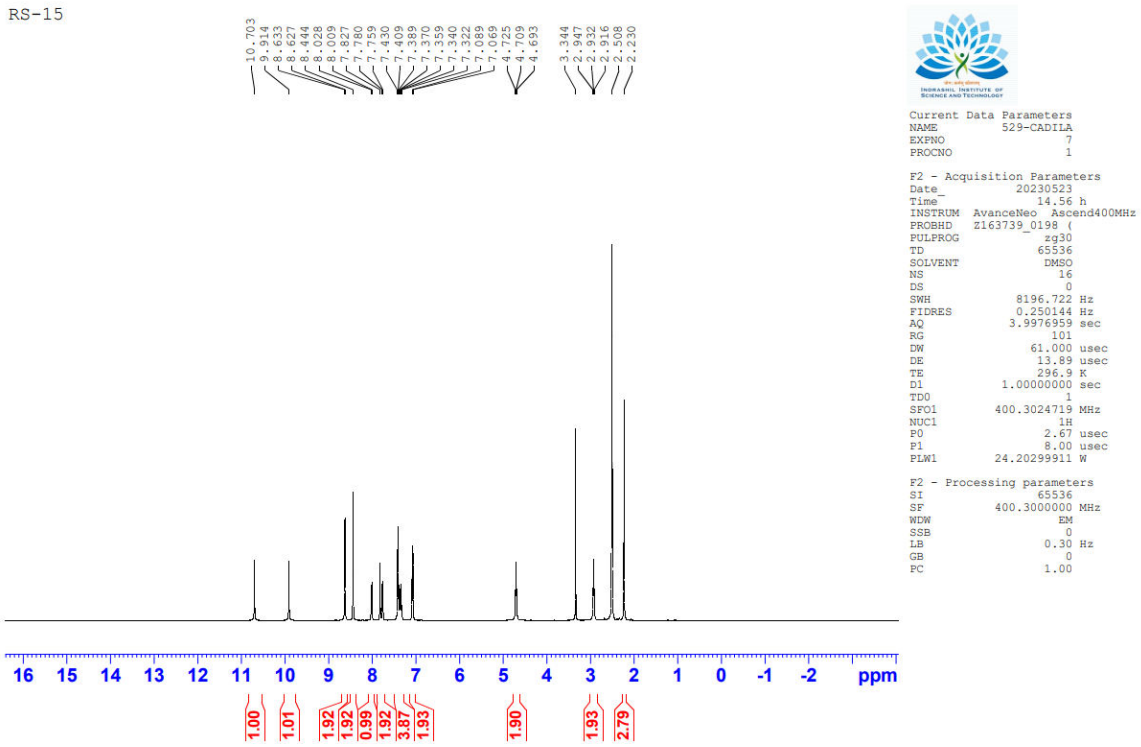

Figure 37: Representative ^{1}H NMR spectrum of compound 9j

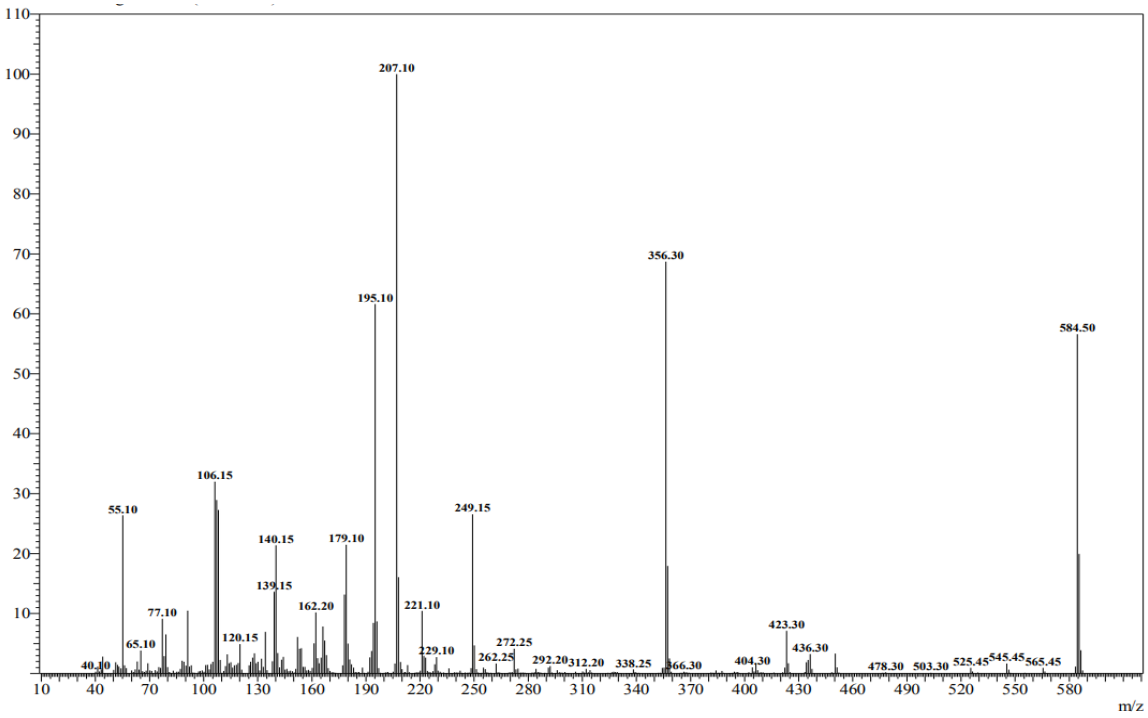

Figure 38: Representative mass spectrum of compound 9j

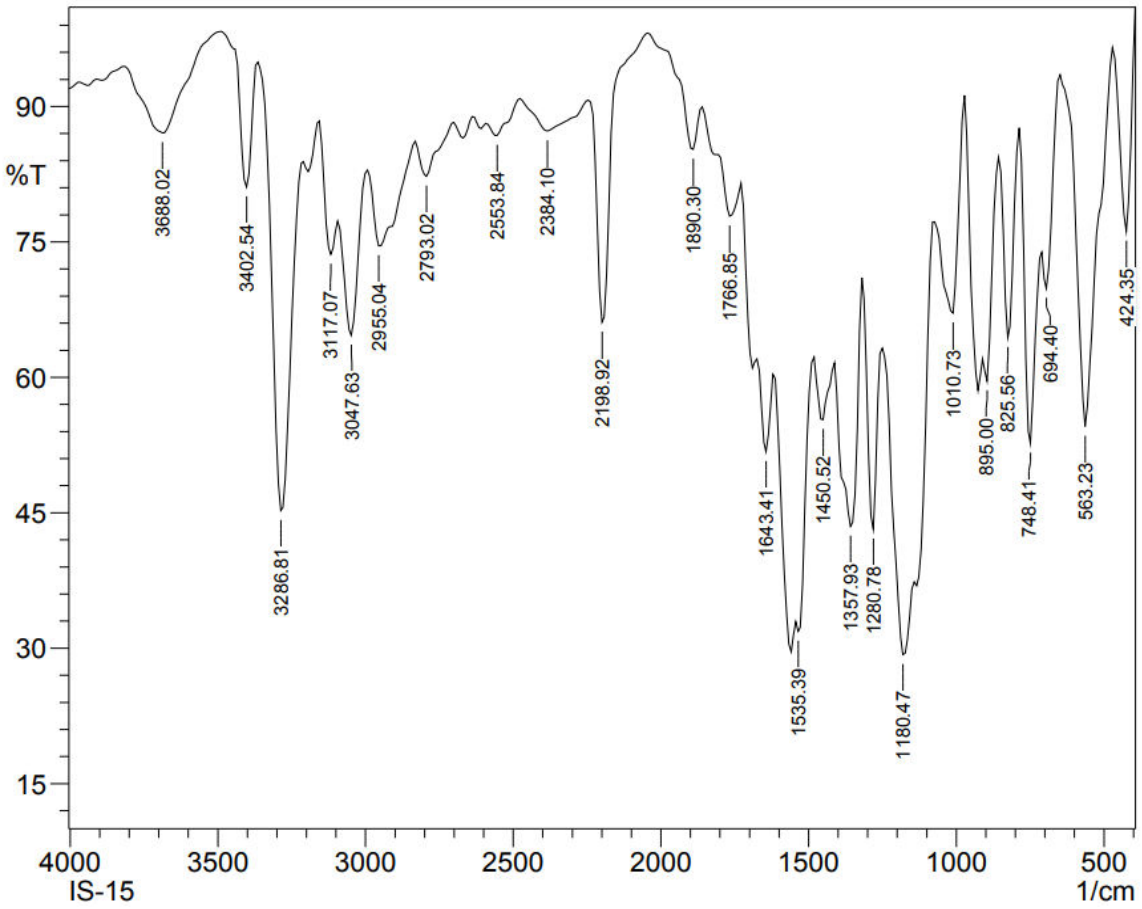

Figure 39: Representative FT-IR spectrum of compound 9j